IMMUNOLOGY

TWIST1 and *TSG6* are coordinately regulated and function as potency biomarkers in human MSCs

Ryang Hwa Lee[1]*, Siddaraju V. Boregowda[2], Taeko Shigemoto-Kuroda[1], EunHye Bae[1], Christopher L. Haga[2], Colette A. Abbery[1], Kayla J. Bayless[1], Andrew Haskell[1], Carl A. Gregory[1], Luis A. Ortiz[3], Donald G. Phinney[2]*

Mesenchymal stem/stromal cells (MSCs) have been evaluated in >1500 clinical trials, but outcomes remain suboptimal because of knowledge gaps in quality attributes that confer potency. We show that TWIST1 directly represses *TSG6* expression that *TWIST1* and *TSG6* are inversely correlated across bone marrow–derived MSC (BM-MSC) donor cohorts and predict interdonor differences in their proangiogenic, anti-inflammatory, and immune suppressive activity in vitro and in sterile inflammation and autoimmune type 1 diabetes preclinical models. Transcript profiling of *TWIST1*^{Hi}*TSG6*^{Low} versus *TWIST*^{Low}*TSG6*^{Hi} BM-MSCs revealed previously unidentified roles for TWIST1/TSG6 in regulating cellular oxidative stress and TGF-β2 in modulating *TSG6* expression and anti-inflammatory activity. *TWIST1* and *TSG6* levels also correlate to donor stature and predict differences in iPSC-derived MSC quality attributes. These results validate *TWIST1* and *TSG6* as biomarkers that predict interdonor differences in potency across laboratories and assay platforms, thereby providing a means to manufacture MSC products tailored to specific diseases.

INTRODUCTION

Mesenchymal stem/stromal cells (MSCs) represent a high-value resource for regenerative medicine applications due to their ability to support hematopoiesis (*1*–*3*), generate osseous tissue (*4*), and release paracrine factors (*5*, *6*) and extracellular vesicles (*7*) in response to environmental cues that promote therapeutic effects. However, while MSC products have been tested in humans for various indications, outcomes have been largely suboptimal, and no MSC-based therapies are currently approved for use in the United States (*8*). A major limitation in development of efficacious MSC-based products with predictable therapeutic indexes in humans is that methods used to isolate cells yield functionally heterogeneous populations (*5*, *9*–*11*), and no industry-wide standards exist for donor selection and manufacturing processes (*12*, *13*). Moreover, in the United States, each MSC investigational new drug application is evaluated on the basis of its individual attributes and not compared to other existing MSC-based products (*8*), which confounds efforts to compare the potency and efficacy of different products in patients. The latter may explain why results from independent clinical trials are largely incongruent (*14*, *15*). This problem is exacerbated by the paucity of metrics available to assess product heterogeneity in terms of both biological function and potency, which hampers efforts to select the most suitable "batch" of MSCs for treating a given disease indication or patient population. Consequently, many clinical studies produce MSCs using similar donor selection and manufacturing processes to treat diseases of unrelated pathogenesis.

To address these limitations, efforts have focused on identifying biomarkers that stratify patients into responders versus nonresponders (*16*) and define MSC products on the basis of potency rather than phenotype or composition of matter. While low-throughput assays that relate potency to quantifiable differences in cell morphology, gene expression, or activity in cell-based assays have been reported, these approaches are limited in scope because they seek to predict the potency or improve efficacy for one class of disease indication. We recently identified *TWIST1* as a biomarker that predicts interdonor differences in stem/progenitor and paracrine activities of bone marrow (BM)–derived MSCs (BM-MSCs) (*17*). TWIST1 is a member of the basic helix-loop-helix family of transcription factors (*18*) and plays important roles in angiogenesis (*19*–*22*), maintenance of hematopoietic stem cells (*23*, *24*) and skeletal muscle progenitors (*25*, *26*), regulation of myeloid lineage determination (*27*), and cytokine signaling (*28*). We showed that *TWIST1* mRNA levels predict interdonor differences in the growth, viability, colony-forming unit–fibroblast (CFU-F) activity, and trilineage differentiation potential of BM-MSCs; that silencing of *TWIST1* down-regulated transcripts encoding proteins with proangiogenic activity and induced those with anti-inflammatory and immunomodulatory activity; and that manipulating *TWIST1* levels predictably altered the capacity of BM-MSCs to support endothelial tubule formation and suppress activated CD3$^+$ T cell proliferation in cell-based assays (*29*). BM-MSCs with disparate *TWIST1* levels were also shown to exhibit predictable differences in anti-inflammatory activity in a mouse model of acute lung injury (*29*). Together, these results indicate that stem/progenitor and paracrine functions of BM-MSCs are mechanistically linked via the action of TWIST1, which we exploited to develop a Clinical Indications Prediction (CLIP) scale that discriminates BM-MSCs on the basis of proangiogenic versus anti-inflammatory/immunomodulatory activity (*17*, *29*). A growing number of independent studies have demonstrated that proangiogenic activity exists at the expense of anti-inflammatory and immune suppressive activities as predicted by our CLIP scale (*30*). We and others have also identified tumor necrosis factor (TNF)–stimulated gene/protein 6

[1]Department of Cell Biology and Genetics, School of Medicine, Texas A&M University, College Station, TX, 77845, USA. [2]Department of Molecular Medicine, The Herbert Wertheim UF Scripps Institute for Biomedical Innovation and Technology, Jupiter, FL, 33458, USA. [3]Department of Environmental Health, University of Pittsburgh, Pittsburgh, PA 15261, USA.
*Corresponding author. Email: dphinney@ufl.edu (D.G.P.); rlee@tamu.edu (R.H.L.)

(TSG6) as an important mediator of MSC anti-inflammatory activity. For example, MSCs were shown to attenuate myocardial infarction–induced cardiac injury (*31*), peritoneal injury (*32*), acute pancreatitis (*33*), and zymosan-induced mouse peritonitis (*34*); reduce colitis (*35*, *36*); and suppress corneal inflammatory lymph angiogenesis (*37*) in a TSG6-dependent manner. Lee *et al.* (*38*) also demonstrated that *TSG6* expression levels exhibit significant interdonor heterogeneity and positively correlate with BM-MSC anti-inflammatory activity in mouse models of sterile inflammation and acute lung injury and negatively correlate with osteogenic potential (*38*). However, whether TWIST1 and TSG6 function independently or are mechanistically linked in BM-MSCs and whether cooperative gene effects enhance the predictive power of each biomarker are indeterminate.

Here, we demonstrate that TWIST1 represses *TSG6* via direct promoter binding, that *TWIST1* and *TSG6* expression are inversely correlated in BM-MSC donor cohorts obtained from different sources and expanded across laboratories, and that these mRNAs predict interdonor differences in BM-MSC potency across assay platforms and preclinical disease models. Transcript profiling of $TWIST1^{Hi}TSG6^{Low}$ versus $TWIST1^{Low}TSG6^{Hi}$ BM-MSCs implicated TWIST1 and TSG6 in regulating cellular oxidative stress responses and demonstrated that transforming growth factor–β2 (TGF-β2) modulates cell size and anti-inflammatory activity by up-regulating *TSG6* expression. Last, we show that *TWIST1* and *TSG6* levels are positively and negatively correlated, respectively, with BM-MSC donor stature. Together, these data validate *TWIST1* and *TSG6* as robust potency biomarkers, confirm a mechanistic link between stem/progenitor and paracrine functions of BM-MSCs, and challenge the paradigm that MSC potency is engendered solely by interaction with the host microenvironment. Our results further highlight the importance of donor screening in clinical trial design, which, to date, has been prejudiced toward optimizing cell yields and provide a rational platform in the form of the CLIP scale to manufacture MSC products tailored to specific disease indications.

RESULTS

TWIST1 and *TSG6* predict interdonor differences in BM-MSC growth, viability, and CFU-F activity

We previously reported that population-averaged expression levels of *TWIST1* and *FGFR2IIIc* positively correlate with growth/viability and CFU-F activity of BM-MSCs sourced from different human donors (*29*). Analysis of a separate donor cohort (RD, $n = 8$) from a commercial vendor revealed significant interdonor differences in population-averaged growth/viability ($F_{7,24} = 37.46$, $P < 0.0001$) and CFU-F activity ($F_{7,40} = 32.32$, $P < 0.0001$; Fig. 1A) and normalized *TWIST1* ($F_{7,38} = 17.76$, $P < 0.0001$) and *FGFR2IIIc* mRNA levels ($F_{7,38} = 59.9$, $P < 0.0001$; Fig. 1B). Regression analysis demonstrated that *TWIST1* and *FGFR2IIIc* mRNA levels positively correlate with cell growth/viability (Fig. 1C) and CFU-F activity (Fig. 1D) and with each other in these donors (Fig. 1E). Analysis of a third donor cohort (BMH, $n = 5$) expanded in human platelet lysate (hPL) supplemented media also exhibited significant interdonor differences in growth/viability ($F_{4,15} = 6.33$, $P = 0.0034$), CFU-F activity ($F_{4,25} = 26.12$, $P < 0.0001$), and *TWIST1* mRNA levels ($F_{4,25} = 15.27$, $P < 0.0001$), and the latter significantly correlated with CFU-F activity in these donors (Fig. 1F). Pooling data from all three donor cohorts evaluated to date revealed a significant positive correlation between *TWIST1* and *FGFR2IIIc* versus CFU-F activity (Fig. 1G), demonstrating the robustness of these relationship across donors. In addition, we found that normalized *TSG6* levels also exhibited significant interdonor variability ($F_{8,46} = 148.6$, $P < 0.0001$; Fig. 1H), consistent with previous reports (*38*), and negatively correlated with *TWIST1* mRNA levels, cell growth/viability, and CFU-F activity (Fig. 1I).

TWIST1 represses *TSG6* expression via direct promoter binding

To explain the observed correlation between *TWIST1* and *TSG6* expressions, we analyzed global chromatin immunoprecipitation sequencing (ChIP-seq) data from BM-MSCs engineered to express a hemagglutinin (HA)–tagged full-length *TWIST1* cDNA (HATW1; GSE220905), which identified HATW1-enriched regions at the *TSG6* gene locus (Fig. 2A). Inspection of these peaks identified four consensus enhancer box (Ebox) motifs within the *TSG6* proximal promoter (Fig. 2B), and ChIP analysis confirmed binding of HATW1 to this region (Fig. 2C). Mutagenesis studies demonstrated that expression of a luciferase reporter cloned downstream of the *TSG6* proximal promoter was significantly up-regulated when Ebox 2 was mutated but not Eboxes 1, 3, or 4 (Fig. 2D). Moreover, small interfering RNA (siRNA)–mediated silencing of *TWIST1* up-regulated *TSG6* expression in BM-MSCs to a significantly greater extent as compared to a scrambled siRNA (Fig. 2E). Treatment of BM-MSCs with the small-molecule harmine (*39*), which inhibited TWIST1 protein expression in a dose-dependent manner (Fig. 2F) without altering *TWIST1* mRNA levels, significantly up-regulated *TSG6* and *IDO1*, a known TWIST1 target, compared to vehicle-treated cells (Fig. 2G). Inhibition of TWIST1 by harmine treatment also enhanced stimulus-directed osteogenic differentiation (Fig. 2H), consistent with studies showing that TWIST1 restrains osteogenic potential (*40*–*43*). Therefore, TWIST1 directly represses *TSG6* expression, thereby providing a mechanistic basis for their orthogonal relationship in all BM-MSCs tested to date.

TWIST1 and *TSG6* predict BM-MSC potency in cell-based and preclinical disease models

To evaluate *TWIST1* and *TSG6* as potency biomarkers, we showed that tubule formation by human umbilical vein endothelial cells (HUVECs) was more highly induced by conditioned medium (CM) from $TWIST1^{Hi}$ ($n = 3$) as compared to $TSG6^{Hi}$ (which are $TWIST1^{Low}$) BM-MSCs ($n = 3$) based on morphometric analysis (Fig. 3A). CM from a $TWIST1^{Hi}$ donor (7052) also stimulated HUVEC invasion into a collagen matrix to a greater extent than a $TSG6^{Hi}$ donor (6015; Fig. 3B). This result is consistent with previous findings showing *TWIST1* induces and represses, respectively, proteins with proangiogenic and angiostatic activity (*29*). Interdonor differences in the ability of BM-MSCs ($n = 13$) to suppress $CD3^+$ T cell proliferation following antibody-mediated activation of peripheral blood mononuclear cells (PBMNCs) (Fig. 3C) also negatively correlated with *TWIST1* and *FGFR2IIIc* and positively correlated with *TSG6* levels (Fig. 3D). To extend these findings to in vivo models, we retrospectively quantified *TWIST1* levels in populations obtained from multiple donors ($n = 7$) whose potency in a sterile inflammation model (Fig. 3E) was shown to be positively correlated with *TSG6* levels (*38*). In these BM-MSCs, *TWIST1* levels

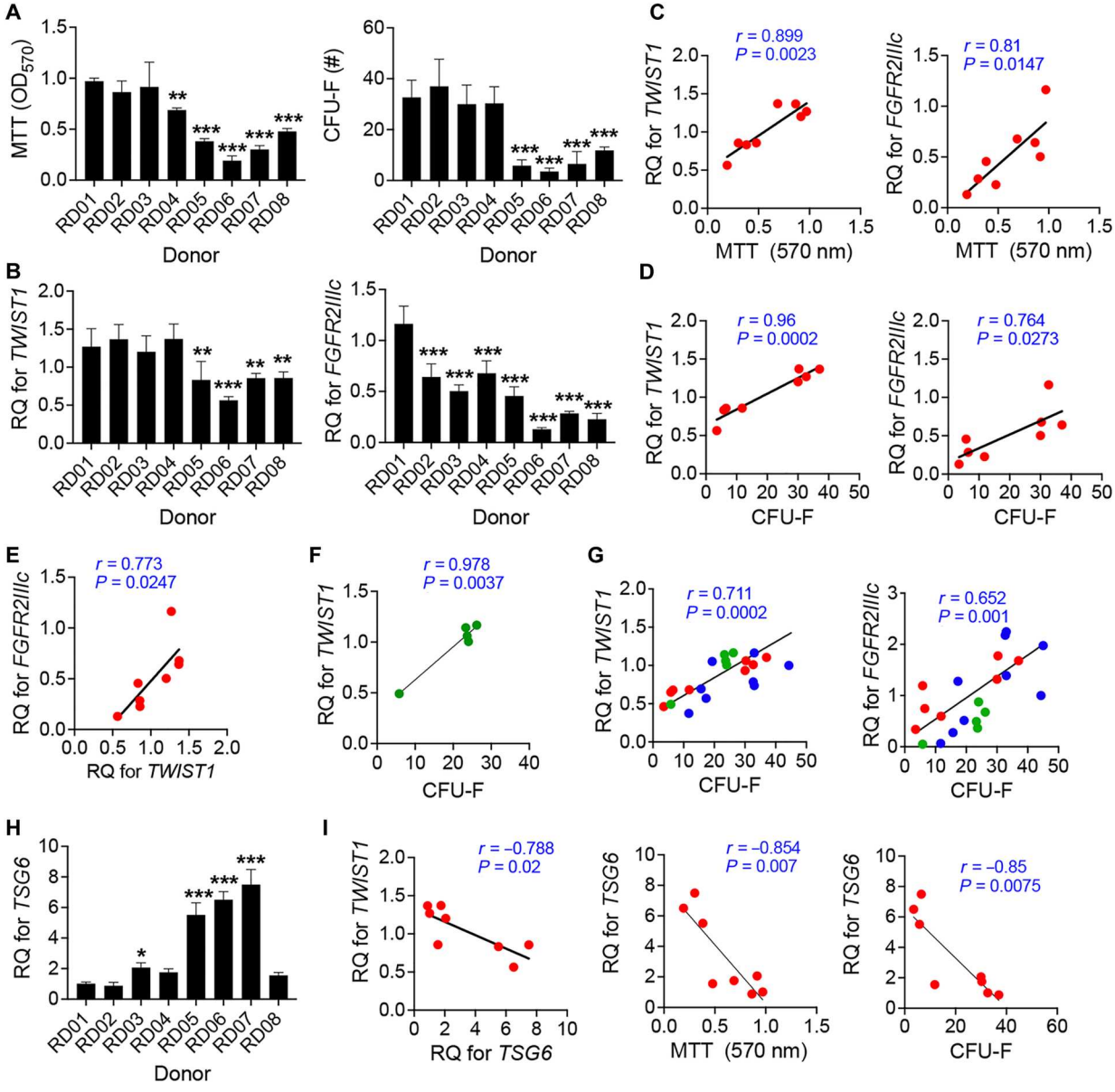

Fig. 1. *TWIST1* and *TSG6* are inversely correlated and predict interdonor differences in BM-MSC attributes. (**A** and **B**) Population-averaged differences in growth/viability and CFU-F activity (A) and *TWIST1*and *FGFR2IIc* mRNA levels (B) in BM-MSCs (n = 8). (**C** and **D**) Scatter plots of *TWIST1*and *FGFR2IIIc* levels versus cell growth/viability (MTT assay) (C) and CFU-F activity (D) in BM-MSCs from (A). (**E**) Scatter plot of *TWIST1* versus *FGFR2IIc* mRNA levels in BM-MSCs from (A). (**F**) Scatter plot of *TWIST1* versus CFU-F activity in BM-MSCs from a separate donor cohort (BHM) expanded in hPL. (**G**) Scatter plots of *TWIST1* and *FGFR2IIIc* versus CFU-F activity based on data pooled from n = 3 donor cohorts [7000: n = 8, blue; RD from (A): n = 8, red; BHM from (F): n = 5, green]. (**H**) Population-averaged differences in *TSG6* mRNA levels in BM-MSCs from (A). (**I**) Scatter plots of *TSG6* versus *TWIST1*, cell growth/viability (MTT), and CFU-F activity in BM-MSCs from (H). Data in (A), (B), and (H) are means ± SD from three to six technical replicates per sample with $^*P < 0.05$, $^{**}P < 0.01$, and $^{***}P < 0.005$ versus RDO1 by one-way analysis of variance (ANOVA) with Tukey post hoc test. Data in (C) to (G) and (I) are means ± SD from four to six technical replicates per sample, and r is the Pearson's product moment correlation coefficient with corresponding P values determined by linear regression. OD_{570}, optical density at 570 nm.

were significantly negatively correlated with *TSG6* mRNA levels (Fig. 3F) and anti-inflammatory activity quantified by reduction of neutrophil levels within the cornea at 24 hours after injury, which predicts corneal opacity at 7 days after injury (Fig. 3G). Using an adoptive transfer model of type 1 diabetes mellitus (T1D), we further assayed the ability of BM-MSCs (n = 7) to prevent T1D onset as defined by two consecutive glycemic measurements of ≥250 mg/dl (Fig. 3H). We confirmed that $TSG6^{Hi}$ (6015, 7012, and 7013) BM-MSCs were more effective in preventing T1D onset in mice compared to those characterized as $TWIST1^{Hi}$ (7052, 7064, and 7074; Fig. 3I). As expected, *TWIST1* expression was negatively correlated with *TSG6* in these BM-MSCs (Fig. 3J), and their potency was negatively correlated with

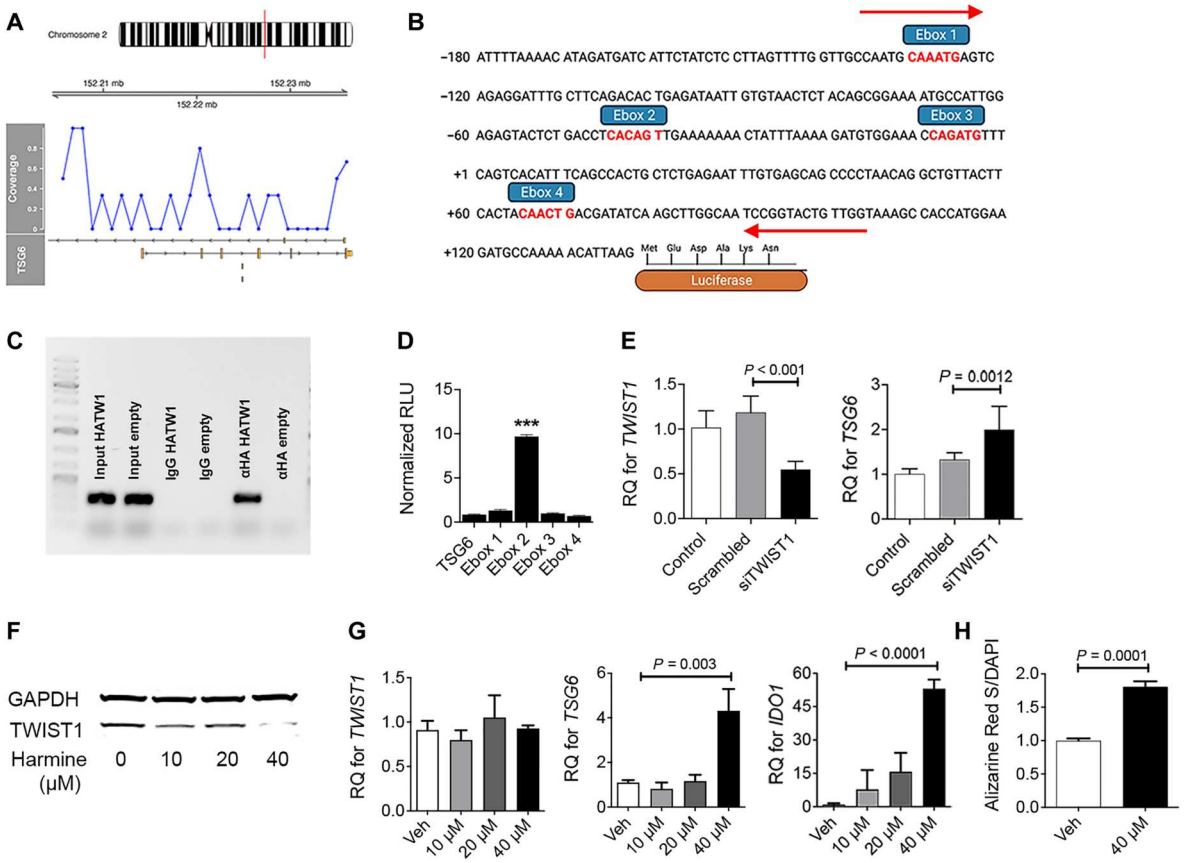

Fig. 2. TWIST1 directly represses *TSG6* expression in BM-MSCs. (**A**) Chromosomal location of the *TSG6* gene (top) (red line) and coverage of HATW1-enriched regions at the *TSG6* locus by ChIP-seq analysis (bottom) (blue peaks). (**B**) Sequence of the *TSG6* proximal promoter where Ebox motifs are indicated by rectangles and their sequences highlighted in red. Arrows are primers used for ChIP-PCR (polymerase chain reaction) analysis in (C). (**C**) Uncropped immunoblot of ChIP-PCR analysis showing pulldown of HATW1 using an anti-HA antibody at the *TSG6* locus in BM-MSCs. (**D**) Normalized luminescence of luciferase reporter driven by the *TSG6* proximal promoter or promoters where the indicated Eboxes were mutated. Data are means ± SD from single experiments with four technical replicates. In Prism, ***$P < 0.005$ versus TSG6 by one-way ANOVA with Tukey post hoc test. (**E**) Quantitative reverse transcription PCR (qRT-PCR) of *TWIST1* and *TSG6* levels in native BM-MSCs and those transfected with a scrambled or *TWIST1*-specific siRNA. Data are means ± SD from biological replicates with four technical replicates per experiment. In Prism, *P* values are by one-way ANOVA with Tukey post hoc test. (**F**) Cropped immunoblot of cell extracts from BM-MSCs pretreated with the indicated concentrations of harmine for 24 hours. (**G**) qRT-PCR of *TWIST1*, *TSG6*, and *IDO1* levels in BM-MSCs from (F). Data are means ± SD from four technical replicates, and *P* values are by one-way ANOVA with Tukey post hoc test. (**H**) Osteogenesis of BM-MSCs pretreated with vehicle or harmine (40 μM). Data are means ± SD from four technical replicates, and the *P* value is by Student's *t* test. IgG, immunoglobulin G; RLU, relative light unit; GAPDH, glyceraldehyde-3-phosphate dehydrogenase; DAPI, 4′,6-diamidino-2-phenylindole.

TWIST1 levels (Fig. 3K) and positively correlated with *TSG6* levels (Fig. 3L).

Lee *et al.* (*38*) previously reported that *TSG6* levels negatively correlate with the height and weight of BM-MSC donors. Reanalysis of these donors showed that *TWIST1* levels positively correlate with donor height (Fig. 4A) and trended higher in male versus female donors (Fig. 4B). To validate this relationship, we generated BM-MSCs from a tall (72 inches) and short (65 inches) male donor of the same race and similar age (25 to 35 years old; Fig. 4C). Analysis of these donor populations revealed that normalized *TWIST1* mRNA levels were significantly higher in BM-MSCs from the tall versus short donor, while *TSG6* levels were significantly higher in BM-MSCs from the short versus tall donor (Fig. 4D). In addition, BM-MSCs from the tall donor were found to exhibit significantly higher growth rates (Fig. 4E) and viability (Fig. 4F) when measured after a single passage and higher CFU-F activity when measured at the end of two consecutive passages (Fig. 4G). These data are consistent with previous results demonstrating that *TWIST1* reliably predicts interdonor differences in BM-MSC fitness (*29*). They also link donor stature to BM-MSC potency as defined by the CLIP scale and hence provide a simple means to prescreen donors to produce products of defined potency.

TWIST1^{Hi}TSG6^{Low} and *TWIST1^{Low}TSG6^{Hi}* BM-MSCs have unique gene signatures

To further interrogate *TWIST1* and *TSG6* function, we compared the transcriptomes of *TWIST1^{Hi}TSG6^{Low}* (group 1; donors 7052, 7064, and 7075) and *TWIST1^{Low}TSG6^{Hi}* (group 2; donors 6015, 7012, and 7013) BM-MSCs by microarray analysis. Unsupervised hierarchical clustering of the top 240 most highly differentially expressed genes (DEGs) segregated populations on their *TWIST1*/*TSG6* status, although one donor from group 1 (7064; G1-21,22) more closely aligned with those from group 2 than its respective group (fig. S1A). Principal components analysis demonstrated

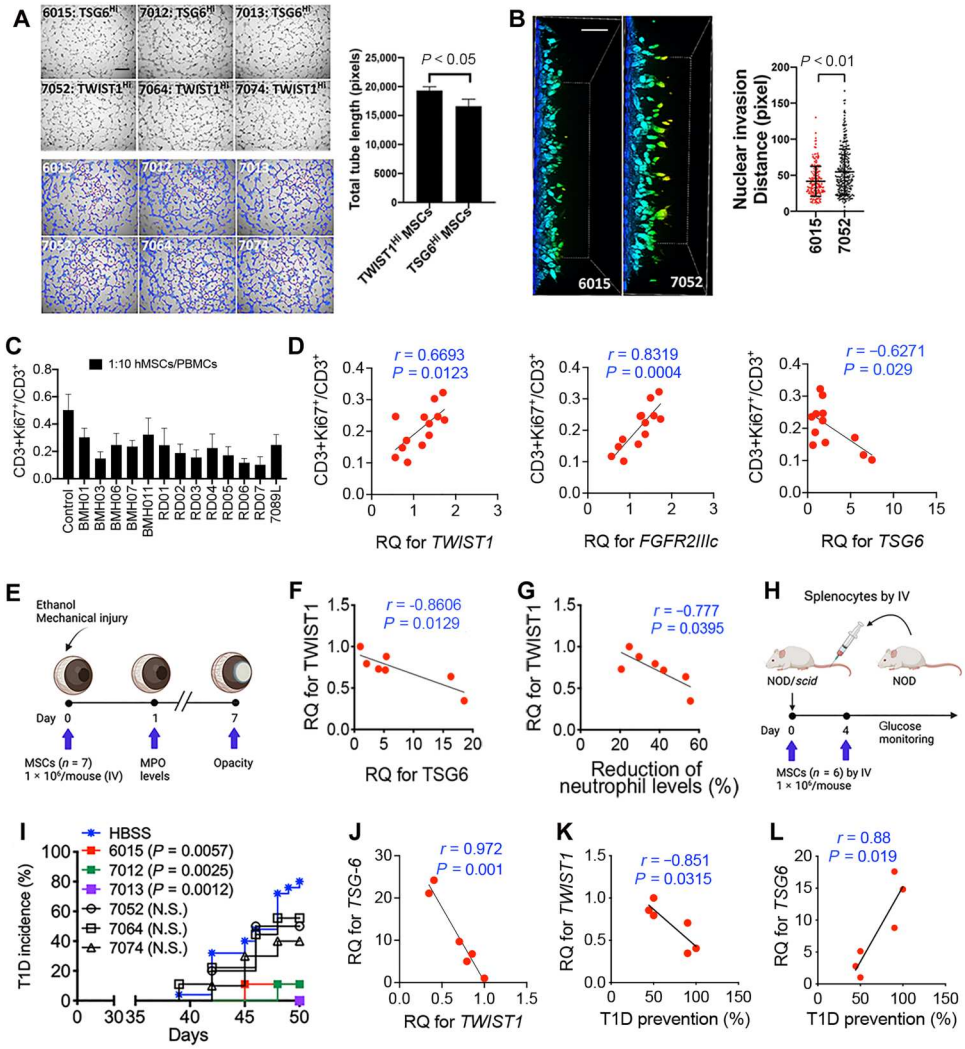

Fig. 3. *TWIST1* and *TSG6* function as potency biomarkers. (**A**) Photomicrographs (top) of HUVECs cultured in CM from the indicated BM-MSCs ($n = 3$ per group) and morphometric analysis (lower) of tubule structures (scale bar, 500 μm). The bar graph shows total tubule length. Data are means ± SD, and P values are by Student's t test. (**B**) Photomicrographs of collagen invasion assay using HUVECs treated with CM from BM-MSCs 6015 and 7052 (scale bar, 100 μm). The bar graph shows nuclear invasion distance. Data are means ± SD, and P values are by Student's t test. (**C**) Ratio of $CD3^+Ki67^+/CD3^+$ PBMNCs in cocultures with the indicated BM-MSCs ($n = 13$) at 4 days after stimulation with anti-CD3/CD28 antibodies. (**D**) Scatter plots of *TWIST1*, *FGFR2IIIc*, and *TSG6* versus $CD3^+Ki67^+/CD3^+$ cells quantified by flow cytometry from assays in (C). Data are means ± SD from biological replicates run in duplicate. (**E**) Schematic of corneal sterile inflammation model wherein myeloperoxidase (MPO) levels measured at 1 day after injury provide a surrogate measure of neutrophil levels and predict corneal opacity at 7 days after injury. (**F** and **G**) Scatter plots of *TWIST1* versus *TSG6* in BM-MSCs (F) ($n = 7$) and reduction in neutrophil levels (G) based on MPO levels in the mouse sterile inflammation model. (**H**) Schematic of the adoptive transfer model of T1D. (**I**) Kaplan-Meier curves of T1D mice administered BM-MSCs [1×10^6 cells, intravenously (IV)] from the indicated donors. The log-rank (Mantel-Cox) test was used to determine P values ($n = 8$ mice per group). (**J** to **L**) Scatter plots of *TWIST1* versus *TSG6* in BM-MSCs administered to mice in (I) and *TWIST1* (K) and *TSG6* (L) versus T1D incidence. r is the Pearson's product moment correlation coefficient with corresponding P values determined by linear regression. N.S., not significant.

that 43.83% and 31.76% of the variation between populations were accounted for by PC1 and PC2, respectively (fig. S1B). This analysis further identified a total of 109 DEGs in $TWIST1^{Hi}TSG6^{Low}$ versus $TWIST1^{Low}TSG6^{Hi}$ BM-MSCs that were altered by $\geq \log_2$ fold change (fig. S1C), of which 36 and 73 were up-regulated in groups 1 and 2, respectively (fig. S1D). On the basis of gene set enrichment analysis (GSEA), these up-regulated DEGs mapped to the cellular component gene ontology (GO) terms "extracellular matrix," "extracellular region," and "extracellular space"; molecular function GO terms involving heparin, carbohydrate, glycosaminoglycan, and polysaccharide binding; and the biological process GO terms "skeletal system development," "positive regulation of T cell activation," "hematopoietic or lymphoid organ development," "positive regulation of leukocyte activation," "oxidation reduction," and Wnt and TGF-β receptor signaling pathways (fig. S1E). We confirmed that transcripts encoding proteins localized to the extracellular space including *TSG6*, *CD24*, *MGP*, *CXCL6*, *FGF7*, *TGF-β2*, and *OXTR* were expressed at significantly higher levels in $TWIST1^{Low}TSG6^{Hi}$ (group 2) versus $TWIST1^{Hi}TSG6^{Low}$ (group 1) BM-MSCs (fig. S1F). These transcripts are known to be up-regulated in response to inflammatory stimuli and encode proteins involved in extracellular remodeling at inflammatory sites,

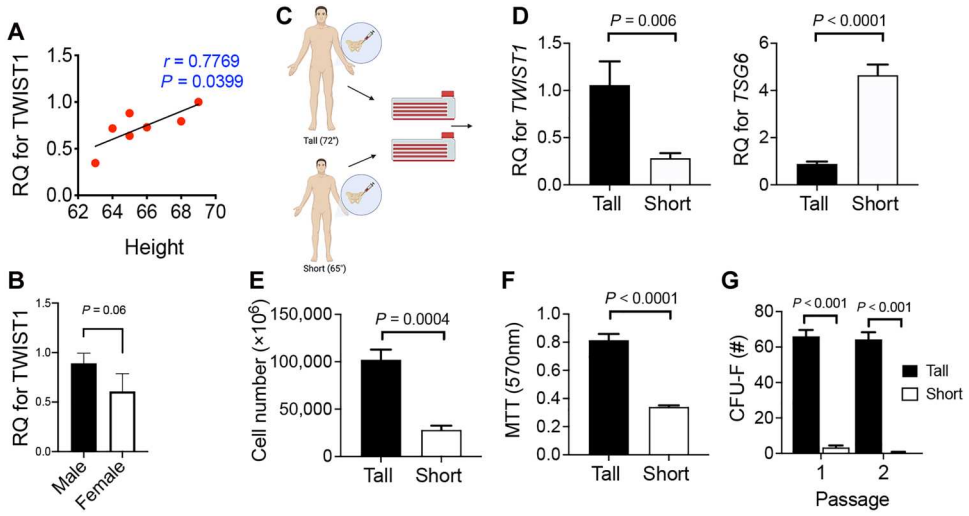

Fig. 4. *TWIST1* correlates with BM-MSC donor stature. (**A** and **B**) Scatter plot of *TWIST1/GAPDH* levels in BM-MSCs versus donor height (A) and bar graph of *TWIST1/GAPDH* levels versus donor sex (B). Data are means ± SD, and *P* values are by Student's *t* test ($n = 7$). (**C**) Schematic showing isolation of BM-MSCs from a tall (72 inches) and short (65 inches) male donor. (**D**) Bar graphs of normalized *TWIST1* and *TSG6* mRNA levels in male donors from (C). Data are means ± SD of three technical replicates, and *P* values are by Student's *t* test. (**E** and **F**) Bar graphs of total cell yield (E) and cell viability (MTT assay) of BM-MSCs from male donors in (C) after a single passage. (**G**) Bar graph of CFU-F activity of BM-MSCs from (C) quantified after each indicated passage. Data in (F) and (G) are means ± SD from four technical replicates, and *P* values are by Student's *t* test.

suppression of immune responses to danger-associated molecular patterns, and regulatory T cell induction, thereby reflecting the potent immunomodulatory activity of *TWIST1*^{Low}*TSG6*^{Hi} BM-MSCs (group 2). Last, we analyzed both BM-MSC cohorts by flow cytometry, which revealed that *TWIST1*^{Low}*TSG6*^{Hi} MSCs (group 2) had significantly larger forward scatter, indicative of larger cell size as compared to *TWIST1*^{Hi}*TSG6*^{Low} BM-MSCs (group 1; fig. S1G). Group 2 BM-MSCs also exhibited larger side scatter, indicative of increased cell complexity, but this difference did not reach statistical significance. Together, these findings demonstrate that *TWIST1*^{Hi} versus *TSG6*^{Hi} BM-MSCs have distinct gene signatures, which mirror differences in their potency in both cell-based and preclinical models (Fig. 3).

TWIST1 and TSG6 modulate oxidative stress responses in BM-MSCs

TWIST1 is known to exhibit antioxidant properties in cancer cells (*44*), and GSEA of up-regulated DEGs in *TWIST1*^{Low}*TSG6*^{Hi} MSCs returned genes associated with oxidation/reduction and response to oxygen levels. To determine whether BM-MSCs from groups 1 and 2 evaluated by microarray exhibit differences in cellular oxidative stress, we subjected representative populations from each group to flow cytometric analysis, which revealed that *TWIST1*^{Low}*TSG6*^{Hi} (6015, G2-11,12) BM-MSCs retained higher intracellular reactive oxygen species (ROS) levels compared to *TWIST1*^{Hi} *TSG6*^{Low} (7052, G1-11,12) BM-MSCs (Fig. 5A). Moreover, while siRNA-mediated silencing of *TWIST1* induced significant increases in total ROS levels in both populations, levels were highest in *TWIST1*^{Low}*TSG6*^{Hi} (6015) BM-MSCs (Fig. 5B), which also exhibited measurable increases in cell size and cellular granularity within 24 hours after treatment (fig. S2A). Silencing of *TWIST1* also induced expression of *TSG6* mRNA in both populations, whereas *TGF-β2* expression was significantly up-regulated only in *TWIST1*^{Low}*TSG6*^{Hi} (6015) BM-MSCs (Fig. 5C). To further assess cellular oxidative stress responses, we cultured these BM-MSCs in varying concentrations of hydrogen peroxide for 24 hours, which revealed clear differences in sensitivity. For example, viability measurements indicated that *TWIST1*^{Hi}*TSG6*^{Low} (7052) BM-MSCs were more resistant to low doses and less resistant to high doses of peroxide as compared to their *TWIST1*^{Low}*TSG6*^{Hi} (6015) counterpart (Fig. 5D). Moreover, low doses of peroxide up-regulated *TWIST1*, and high doses up-regulated *TSG6* and *TGF-β2* expression in *TWIST1*^{Low}*TSG6*^{Hi} (6015) BM-MSCs, whereas *TWIST1* and *TGF-β2* expression were largely unaffected by peroxide treatment, and *TSG6* expression was only modestly induced by high peroxide doses in *TWIST1*^{Hi}*TSG6*^{Low} (7052) BM-MSCs (Fig. 5E). TGF-β2 is induced in response to oxidative stress (*45*) and protects cells from free radical–mediated injury (*46*), which may explain the increased resistance of *TWIST1*^{Low} *TSG6*^{Hi} BM-MSCs to oxidative stress. To determine whether TSG6 affords similar protection, we silenced its expression in *TWIST1*^{Low} *TSG6*^{Hi} (6015) BM-MSCs, which resulted in significant increases in cell size based on morphology (fig. S2B) and forward and side scatter based on flow cytometric analysis (Fig. 5F). It also induced significant increases in *TGF-β2*, but not *TWIST1* (Fig. 5F). Other genes that track with *TGF-β2* including *CXCL6* and *OXTR* were also induced to significant levels (fig. S2B). Alternatively, overexpression of TSG6 in *TWIST1*^{Low}*TSG6*^{Hi} reverted cells to a *TWIST1*^{Hi}*TSG6*^{Low}-like morphology (fig. S2C), induced measurable decreases in cell size and cellular granularity, and down-regulated expression of *TGF-β2* but did not significantly alter expression of *TWIST1* (Fig. 5G). *OXTR* levels were also significantly down-regulated as expected (fig. S2C). To confirm these observations, we analyzed two additional BM-MSC donors from the microarray studies, which confirmed that *TWIST1*^{Low}*TSG6*^{Hi} (7012) BM-MSCs retained higher cellular ROS levels compared to their *TWIST1*^{Hi}*TSG6*^{Low} (7074) counterpart (fig. S2D). Silencing of *TWIST1* in these donors also yielded similar impacts on *TSG6* and

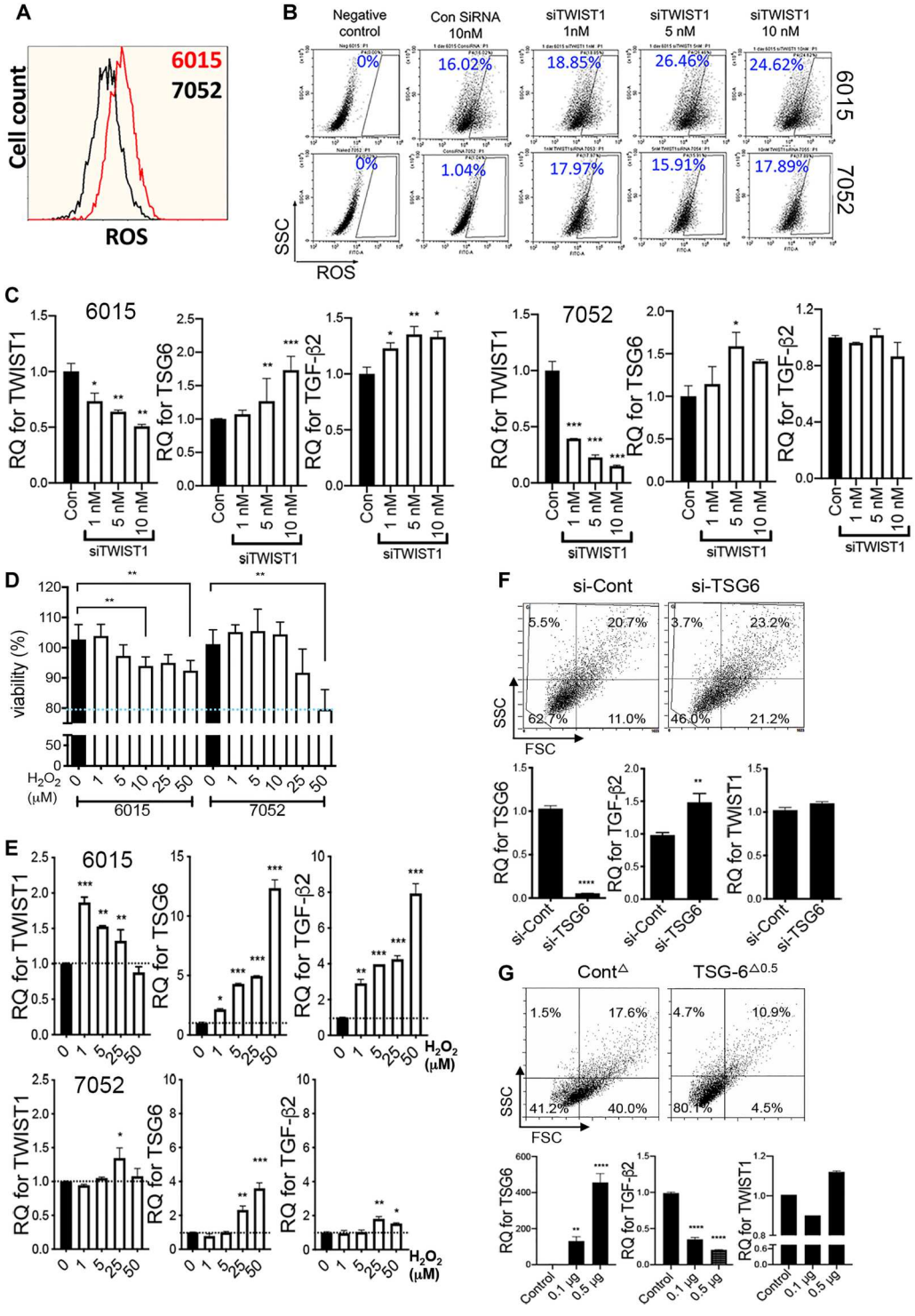

Fig. 5. Impacts of TWIST1, TSG6, and TGF-β2 on cellular ROS levels and oxidative stress responses in BM-MSCs. (**A**) Histogram of cellular ROS levels in *TWIST1*^{Hi}*TSG6*^{Low} (7052) and *TWIST1*^{Low} *TSG6*^{Hi} (6015) BM-MSCs quantified by flow cytometric analysis. (**B**) Dot plots from flow cytometric analysis of ROS levels in native and *TWIST1*-specific siRNA-transfected BM-MSCs from (A). (**C**) qRT-PCR quantification of normalized *TWIST1*, *TSG6*, and *TGF-β2* levels in BM-MSCs from (B). Data are means ± SD from triplicates. **P* < 0.05, ***P* < 0.01, and ****P* < 0.005 versus control by one-way ANOVA with Dunnett's multiple comparisons test. (**D**) Cell viability of *TWIST1*^{Hi}*TSG6*^{Low} (7052) and *TWIST1*^{Low}*TSG6*^{Hi} (6015) BM-MSCs at 24 hours after exposure to the indicated doses of hydrogen peroxide. Data are means ± SD of triplicates. ***P* < 0.01 by one-way ANOVA with Dunnett's multiple comparisons test. (**E**) qRT-PCR quantification of normalized *TWIST1*, *TSG6*, and *TGF-β2* levels in BM-MSCs from (D). Data are means ± SD from triplicates. **P* < 0.05, ***P* < 0.01, and ****P* < 0.005 versus untreated cells by one-way ANOVA with Dunnett's multiple comparisons test. (**F**) Representative dot plots from flow cytometric analysis (top) and qRT-PCR quantification of *TSG6*, *TGF-β2*, and *TWIST1* levels (bottom) in *TWIST1*^{Low}*TSG6*^{Hi} BM-MSCs (6015) at 24 hours after transfection with a scrambled or *TSG6*-specific siRNA (10 mM). Data are means ± SD from triplicates. ***P* < 0.01 and *****P* < 0.001 by Student's *t* test. (**G**) Representative dot plots from flow cytometric analysis (top) and qRT-PCR quantification of *TSG6*, *TGF-β2*, and *TWIST1* (bottom) levels in *TWIST1*^{Low} *TSG6*^{Hi} in BM-MSCs (6015) at 24 hours after transfection with a control or TSG6 plasmid (0.1 to 0.5 mg/cm^2). Data are means ± SD from triplicates. ***P* < 0.01 and *****P* < 0.001 versus control by one-way ANOVA with Dunnett's multiple comparisons test.

TGF-β2 expression levels (fig. S2E) and induced measurable increases in cell size and granularity (fig. S2F). Last, silencing and overexpression of TSG6 in *TWIST1*^{Low}*TSG6*^{Hi} (7012) BM-MSCs increased and reduced cell size, respectively, on the basis of morphological and flow cytometric analysis as expected (fig. S2, G and H). These results are consistent with our previous observations that modest overexpression of TSG6 in *TWIST1*^{HI}*TSG6*^{low} enhanced their anti-inflammatory activity in a murine model of corneal injury (*38*), but superphysiological levels failed to improve therapeutic potency in this model (fig. S3). They also suggest that the ability to transiently up-regulate *TSG6* and *TGF-β2* affords *TWIST1*^{Low}*TSG6*^{Hi} BM-MSCs greater protection against oxidative stress.

TGF-β2 alters BM-MSC anti-inflammatory activity in vivo

TGF-β is a profibrotic cytokine (*47*) that modulates expression of extracellular matrix proteins (*48*). Our transcript profiling data indicate that *TGF-β2* expression tracks with *TSG6* (fig. S1F) and both transcripts are induced in BM-MSCs by cellular oxidative stress (Fig. 5E). TGF-β2 has been reported to both enhance (*49*, *50*) or impair (*51*) the anti-inflammatory activity of murine BM-MSCs. We showed that *TWIST1*^{Low}*TSG6*^{Hi} (6015) BM-MSCs secrete significantly higher levels of TGF-β2 compared to *TWIST1*^{Hi}*TSG6*^{Low} (7052) cells, which we confirmed by extending this analysis to several additional BM-MSC populations used in the microarray studies (Fig. 6A). We further demonstrated that siRNA-mediated silencing of TGF-β2 in *TWIST1*^{Low}*TSG6*^{Hi} (6015) BM-MSCs significantly decreased *TSG6* mRNA levels (Fig. 6B) and augmented osteogenic differentiation (fig. S4A). Treatment of *TWIST1*^{Low} *TSG6*^{Hi} (6015) BM-MSCs with the TGFBR1 inhibitor SB431542 (*52*) decreased *TGF-β2*, *TSG6*, and *OXTR* mRNA levels while increasing *TWIST1* levels (Fig. 6C). Alternatively, treatment of *TWIST1*^{Hi}*TSG6*^{Low} BM-MSCs (7052) with 50 or 200 pg/ml of recombinant human TGF-β2 resulted in significant increases in forward and side scatter based on flow cytometric analysis (Fig. 6D) and up-regulated expression of *TSG6*, *OXTR*, and *CXCL6* mRNAs in a dose-dependent manner (Fig. 6E). However, *TWIST1* expression was significantly induced by 50 pg/ml but not 200 pg/ml of TGF-β2 in this donor (Fig. 6E). Treatment of a second *TWIST1*^{Hi}*TSG6*^{Low} (7074) population with TGF-β2 resulted in similar impacts on cell size (Fig. 6F) and *TSG6* and *OXTR* expression (Fig. 6G), but in this donor, *TWIST1* levels were decreased (Fig. 6G). Last, we found that diabetes incidence was significantly reduced in mice administered *TWIST1*^{Hi}*TSG6*^{Low} BM-MSCs (7052) pretreated with TGF-β2 (200 pg/ml) as compared to mice administered naïve, nontreated cells (Fig. 6H). TGF-β2 also decreased the osteogenic potential of *TWIST1*^{Hi}*TSG6*^{Low} BM-MSCs (7052; fig. S4B). Together, these data indicate that TGF-β2 induces *TSG6* and alters the size, granularity, osteogenic potential, and anti-inflammatory activity of BM-MSCs in a manner antagonistic to TWIST1.

TWIST1 and *TSG6* expression predicts functional attributes of induced pluripotent stem cell–derived MSCs

Several studies have shown that MSCs can be generated from induced pluripotent stem cells (iPSCs) by treatment with the TGF-β inhibitor SB431542 (*53*–*55*) and that these iPSC-derived MSCs (iPSC-MSCs) exhibit greater osteogenic capacity compared to BM-MSCs (*56*). Consistent with these findings, we found that these iPSC-MSCs expressed ~8-fold higher *TWIST1* levels compared to *TWIST1*^{Hi}*TSG6*^{Low} (7052) BM-MSCs and ~10-fold lower *TSG6* levels compared to *TWIST1*^{Low}*TSG6*^{Hi} (6015) BM-MSCs (Fig. 7A). Flow cytometric analysis (Fig. 7B) further demonstrated that iPSC-MSCs exhibit lower forward and side scatter than *TWIST1*^{Hi}*TSG6*^{Low} (7052) BM-MSCs (Fig. 7C), which is consistent with their higher growth rate. Previously, we demonstrated that *TSG6*^{Hi} but not *TSG6*^{Low} BM-MSCs effectively suppressed the proinflammatory mediators TNF-α, CXCL1, and CXCL2 in peritoneal lavage of mice challenged with Zymosan A (*38*). iPSC-MSCs (1.5×10^6 cells) administered to mice challenged with Zymosan A were also ineffective in reducing expression of TNF-α, CXCL1, and CXCL2 in peritoneal lavage, whereas dexamethasone administration, which served as a positive control, significantly attenuated Zymosan A–induced inflammation in mice (Fig. 7D). Recently, we observed that microcarrier culture conditions improved the anti-inflammatory activity of iPSC-MSCs (personal communication). Consistent with this observation, we found that these culture conditions increase *TSG6* and decrease *TWIST1* expression levels in cells (Fig. 7E). In addition, when iPSC-MSCs were expanded in a hollow-fiber bioreactor system, they expressed higher levels of *TSG6* than *TWIST1*^{Hi}*TSG6*^{Low} BM-MSCs (Fig. 7F), and similar to BM-MSCs, these iPSC-MSCs significantly suppressed sterile inflammation responses and reduced corneal opacity in a TSG6-dependent manner (*57*). Last, we found that treatment of iPSC-MSCs with recombinant human TGF-β2 significantly decreased *TWIST1* levels and increased *TSG6* levels in a dose-dependent manner (Fig. 7G) while decreasing osteogenic potential (Fig. 7, H and I). Collectively, these data indicate that *TWIST1* and *TSG6* expression levels also predict differences in the potency of iPSC-MSCs, further expanding and validating their utility as potency biomarkers.

DISCUSSION

Implicit in the design of MSC-based clinical therapies is the need to generate large numbers of cells to achieve recommended patient doses. Consequently, most clinical manufacturing protocols select for MSC populations that exhibit robust growth or augment growth by culturing cells in proprietary medium supplements. As a result, it is commonplace to use similar manufacturing regimens to produce MSC products for treating medically unrelated disease indications. These well-established practices have deemphasized the need to stratify MSC populations on the basis of donor characteristics, and while efforts to develop assays that predict product efficacy remains a key focus for the field, these are not linked to donor selection criteria. In this study, we identify key attributes of *TWIST1* and *TSG6* that validate their utility as biomarkers to predict interdonor differences in MSC potency across platforms and disease indications. First, we show that TWIST1 directly represses *TSG6* expression and that expression of these mRNAs are inversely correlated across multiple BM-MSC human donor cohorts sourced from different providers and expanded in different laboratories (Fig. 8). Therefore, this correlation is highly robust. Second, we show that population-averaged, normalized levels of *TWIST1* and *TSG6* predict interdonor differences in BM-MSC potency in both cell-based assays and preclinical disease models (Fig. 8). Because *TWIST1* levels also correlate with CFU-F activity, this relationship provides an internal "standard" to stratify populations based on potency using our previously described CLIP scale (*29*). Third, outcomes from both cell-based assays and animal models reveal clear interdonor differences in BM-MSC potency and hence challenge the existing paradigm that potency is determined by interaction with the host microenvironment in vivo. While our studies do not rule out a role for the host microenvironment, they clearly demonstrate that donor-dependent differences in potency predict therapeutic efficacy in preclinical disease models independent of the host microenvironment. Fourth, we show that *TWIST1* and *TSG6* correlate with donor stature and that BM-MSCs from tall- versus short-statured donors exhibit intrinsic differences in behavior (Fig. 8). These results are consistent with observed interdonor differences in potency and suggest that genetic or epigenetic factors may contribute to such differences. Several genetic alterations

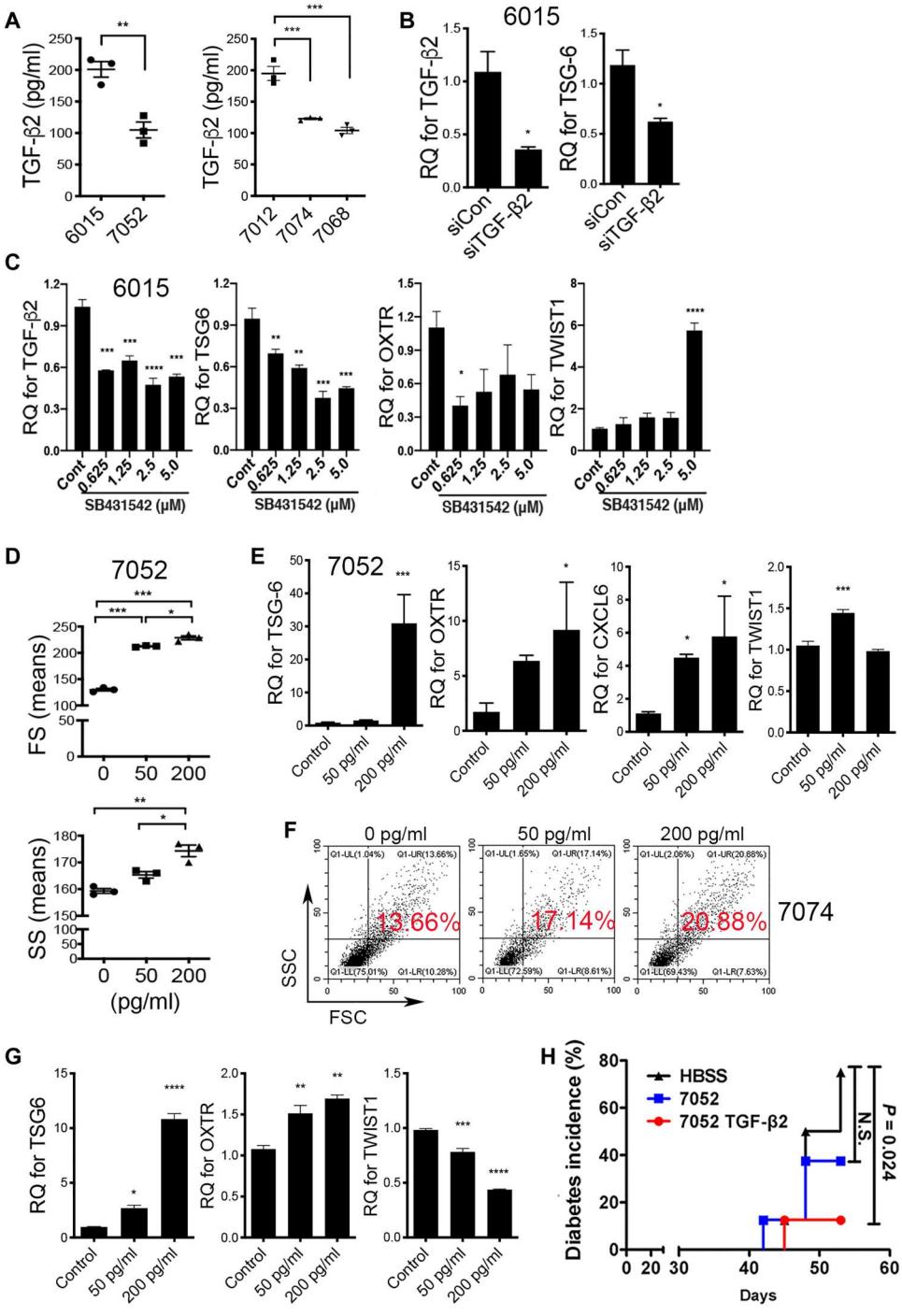

Fig. 6. TGF-β2 modulates BM-MSC cell size, osteogenic capacity, and anti-inflammatory activity. (**A**) Enzyme-linked immunosorbent assay (ELISA) of TGF-β2 in CM from *TWIST1*^{Low}*TSG6*^{Hi} (left, 6015; right, 7012) and *TWIST1*^{Hi} *TSG6*^{Low} (left, 7052; right, 7074 and 7068) BM-MSCs. Data are means ± SD from triplicates, and $^{**}P < 0.01$ is by Student's *t* test. (**B**) qRT-PCR quantification of *TGF-β2* and *TSG6* levels in *TWIST1*^{Low}*TSG6*^{Hi} (6015) BM-MSCs at 48 hours after transfection with a control or *TGF-β2*-specific siRNA. Data are means ± SD from triplicates, and $^{*}P < 0.05$ is by Student *t* test. (**C**) qRT-PCR quantification of *TGF-β2*, *TSG6*, *OXTR*, and *TWIST1* levels in *TWIST1*^{Low}*TSG6*^{Hi} BM-MSCs (6015) cultured with or without the indicated concentrations of SB431542 for 4 days. Data are means ± SD from triplicates. $^{*}P < 0.05$, $^{**}P < 0.01$, $^{***}P < 0.005$, and $^{****}P < 0.001$ by one-way ANOVA versus Cont with Dunnett's multiple comparisons test. (**D**) Bar graphs showing average mean forward scatter (FSC) and side scatter (SSC) of *TWIST1*^{Hi}*TSG6*^{Low} BM-MSCs (7052) cultured in the absence or presence of recombinant human TGF-β2 (50 or 200 pg/ml) for 4 days. Data are means ± SD from triplicates. $^{*}P < 0.05$, $^{**}P < 0.01$, and $^{***}P < 0.005$ versus untreated by one-way ANOVA with Tukey post hoc test. (**E**) qRT-PCR quantification of *TSG6*, *OXTR*, *CXCL6*, and *TWIST1* in BM-MSCs from (D). Data are means ± SD from triplicates. $^{*}P < 0.05$ and $^{***}P < 0.005$ versus Cont by one-way ANOVA with Dunnett's multiple comparisons test. (**F** and **G**) Flow cytometry dot plots (F) and qRT-PCR quantification of *TSG6*, *OXTR*, and *TWIST1* levels (G) in *TWIST1*^{Hi}*TSG6*^{Low} BM-MSCs (7074) treated as in (D). Data are means ± SD from triplicates. $^{*}P < 0.05$, $^{**}P < 0.01$, and $^{***}P < 0.005$ versus untreated by one-way ANOVA with Tukey post hoc test. (**H**) Diabetic incidence in nonobese diabetic (NOD)/*scid* mice after transfer of diabetogenic splenocytes and/or *TWIST1*^{Hi} *TSG6*^{Low} BM-MSCs (7052) (1×10^6 cells per mouse) pretreated for 4 days with or without TGF-β2 (200 pg/ml). The log-rank (Mantel-Cox) test was used to determine *P* values ($n = 8$ mice per group).

including single-nucleotide polymorphisms have been identified at the *TWIST1* locus that are associated with susceptibility to breast cancer (*58*), prognosis in gastric cancer (*59*), and osteoporosis (*60*). Fifth, while our studies focused on BM-MSCs, we show that these relationships extend to iPSC-MSCs, which were found to express significantly higher and lower *TWIST1* and *TSG6* levels, respectively, as compared to BM-MSCs, and exhibit weak anti-inflammatory activity in vivo when expanded in monolayers as predicted by the CLIP scale. Moreover, culture-dependent (microcarrier or bioreactor) alterations in *TWIST1* and *TSG6* levels correlated with changes in iPSC-MSC anti-inflammatory activity in vivo. In this regard, we have observed that bioreactor-induced sheer stress serves as a potent inducer of *TSG6* in BM-MSCs similar to oxidative stress and that this induction occurs, in part, because of down-regulation of TWIST1.

Our data also define a unique TWIST1/TGF-β2/TSG6 signaling axis in BM-MSCs. Specifically, we found that *TWIST1*^{Hi}*TSG6*^{Low} and *TWIST1*^{Low}*TSG6*^{Hi} populations exhibit unique gene signatures,

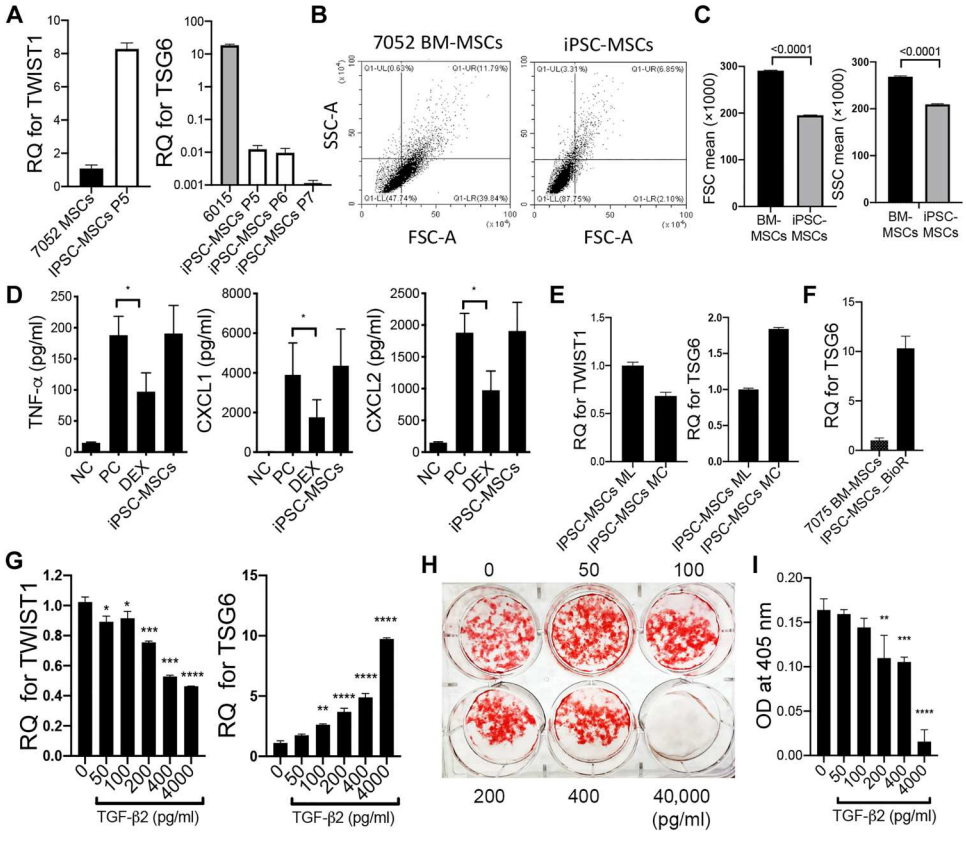

Fig. 7. *TWIST1* and *TSG6* expression predicts functional attributes of iPSC-MSCs. (**A**) qRT-PCR quantification of *TWIST1* and *TSG6* levels in BM-MSCs (7052 or 6015) and iPSC-MSCs at the indicated passage. Data are means ± SD from triplicates. (**B** and **C**) Representative dot plots (B) from flow cytometry analysis of BM-MSCs (7052) and iPSC-MSCs and bar graphs (C) of mean FSC and SSC values. Data are means ± SE from flow cytometry analysis, and *P* values are by Student's *t* test. (**D**) ELISA of TNF-α, CXCL1, and CXCL2 levels in peritoneal lavage from mice (n = 4 to 6 per group) at 4 hours after challenge with Zymosan A [1 mg/mouse, intraperitoneally (IP)]. Mice were administered phosphate-buffered saline (PBS; positive control; PC), dexamethasone (Dex; 1.5 mg/kg, IP), or iPSC-MSCs (1.5×10^6 per mouse, IP) at 15 min after challenge. NC, negative control. Data are means ± SD, and $^*P < 0.05$ is by one-way ANOVA with Tukey post hoc test. (**E**) qRT-PCR quantification of *TWIST1* and *TSG6* levels in iPSC-MSCs grown in monolayer (ML) cultures or on microcarriers (MC) for 8 days. Data are means ± SD from triplicates. (**F**) qRT-PCR quantification of *TSG6* levels in *TWIST1*^{Hi}*TSG6*^{Low} BM-MSCs (7075) grown in ML cultures and iPSC-MSCs grown in a hollow-fiber bioreactor system (Quantum system, Terumo). (**G**) qRT-PCR quantification of *TWIST1* and *TSG6* levels in iPSC-MSCs at 6 days after treatment with the indicated concentrations of TGF-β2. $^*P < 0.05$, $^{**}P < 0.01$, $^{***}P < 0.005$, and $^{****}P < 0.001$ versus untreated cells by one-way ANOVA with Dunnett's multiple comparisons test. (**H**) Alizarin Red S staining of iPSC-MSCs pretreated for 6 days with or without TGF-β2 then cultured for 11 days in osteogenic induction media. (**I**) Quantification of staining data from (H). $^{**}P < 0.01$, $^{***}P < 0.005$, and $^{****}P < 0.001$ versus untreated cells by one-way ANOVA with Dunnett's multiple comparisons test.

express significantly different intracellular ROS levels, and have different sensitivities to oxidative stress induced by peroxide exposure (Fig. 8). Therefore, *TWIST1* and *TSG6* predict not only interdonor differences in potency but also differences in physical (cell size/granularity) and metabolic (ROS generation) parameters. In the latter case, increased resistance of *TWIST1*^{Low}*TSG6*^{Hi} BM-MSCs to oxidative stress was linked to up-regulation of *TGF-β2* and *TSG6* expression in response to such stress, which protect cells from free radical–induced injury and oxidative stress–induced apoptosis (Fig. 8). Stress-induced up-regulation of other extracellular matrix and inflammatory modulators are consistent with the stromal-like phenotype of these cells and their enhanced anti-inflammatory activity in vivo. Alternatively, *TWIST1*^{Hi} *TSG6*^{Low} BM-MSCs maintain low ROS levels, which itself may act as a second messenger to promote stem/progenitor self-maintenance including rapid growth, high CFU-F activity, and multipotency. Continued proliferation of these cells under conditions of oxidative stress likely enhances oxidative damage, which manifests as increased sensitivity to high peroxide doses. These results are consistent with previous studies showing that BM-MSCs cultured in atmospheric oxygen exhibit stress-induced impairments in mitochondrial function (*61*). Last, we previously reported that TWIST1 confers osteogenic potential while restraining osteogenic differentiation in BM-MSCs and that its silencing enhances the latter (*29*). Here, we show that *TGF-β2* suppresses osteogenic differentiation of BM-MSCs, particularly at high doses, while simultaneously repressing *TWIST1* expression in BM-MSCs (Fig. 6) and iPSC-MSCs (Fig. 7). Therefore, *TGF-β2* at low doses may stimulate osteogenic differentiation via TWIST1 down-regulation and, at higher doses, inhibit differentiation independent of TWIST1.

In summary, our findings have important implications regarding the clinical manufacture of BM-MSCs. Our data indicate that populations selected on the basis of rapid growth will be characterized as *TWIST1*^{Hi}*TSG6*^{Low} and exhibit a proangiogenic phenotype.

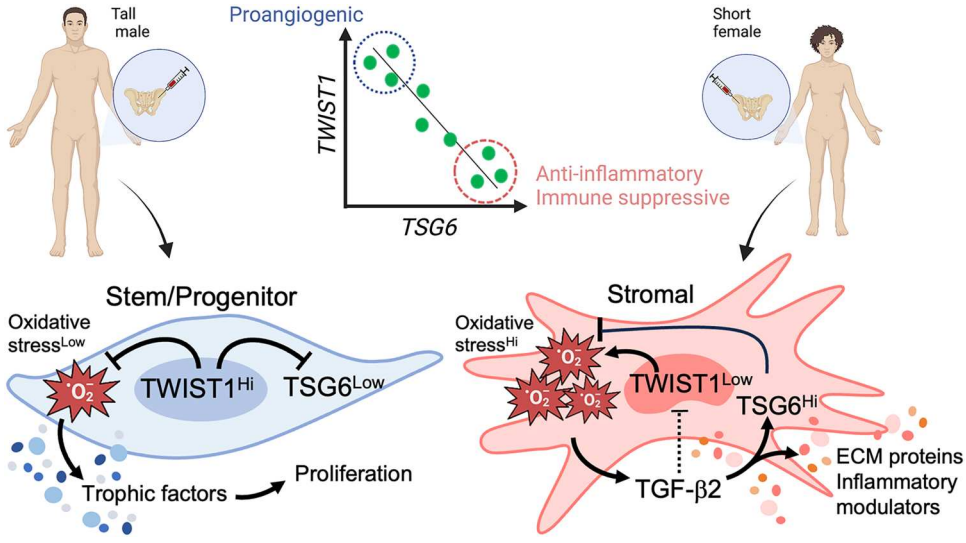

Fig. 8. *TWIST1* and *TSG6* function as potency biomarkers and modulators of cellular oxidative stress in BM-MSCs. *TWIST1* and *TSG6* expression levels are inversely correlated in BM-MSC populations and predict interdonor differences in proangiogenic versus anti-inflammatory/immune suppressive activities in cell-based assays and preclinical disease models. *TWIST1* also positively correlates with the height and sex of BM-MSC donors, while *TSG6* negatively correlates with these attributes. Profiling studies further indicate that $TWIST1^{Hi}TSG6^{Low}$ and $TWIST1^{Low}TSG6^{Hi}$ BM-MSCs exhibit varying sensitivities to oxidative stress and that the latter population up-regulates *TGF-β2*, *TSG6*, extracellular matrix (ECM) proteins, and other inflammatory modulators in response to high levels of such stress, which confers resistance and enhanced anti-inflammatory activity in vivo. Created with BioRender.com.

On the basis of our CLIP scale (*17*, *29*), these cells are appropriate for treating ischemic-related diseases and suboptimal for acute/chronic inflammatory and immune-mediated disorders. Generally, this prediction is consistent with studies demonstrating a clinical benefit of MSC-based therapies in patients with heart disease (*62*–*65*) and a lack of benefit in those with acute inflammatory disorders, such as acute respiratory distress syndrome (*66*–*68*). Le Blanc *et al.* (*69*) demonstrated that BM-MSCs minimally expanded by plating at high density (4000 cells/cm^2) afforded a clinical benefit in patients with steroid refractory graft-versus-host disease (GvHD), and subsequent studies have shown that MSCs are most effective in treating pediatric GvHD patients (*70*, *71*). However, patients with acute or chronic GvHD show lower response rates to treatment with MSCs expanded in human platelet lysate as compared to fetal bovine serum (*72*, *73*). These data are consistent with our observation that BM-MSCs expanded in hPL express high *TWIST1* levels (Fig. 1F). Similarly, McKinnirey *et al.* (*74*) reported that female versus male MSCs were more potent in suppressing PBMNC proliferation in vitro because of their higher expression of Indoleamine 2,3-dioxygenase 1 (IDO1), Interleukin 1 receptor antagonist (IL1RN), and prostaglandin E_2. These findings are consistent with our studies showing that MSCs derived from short-statured or female donors express higher basal and induced levels of TSG6, exhibit more potent anti-inflammatory activity in a sterile inflammation model (*38*), and express low levels of *TWIST1*. Numerous studies have also reported that preconditioning MSCs with cytokines, such as TNF and INFG, enhances their anti-inflammatory and immune suppressive activities (*75*, *76*), which is also consistent with our studies showing that TWIST1 is a target of INFG action in BM-MSCs (*29*) and that pretreatment with TGF-β2 licenses the immune suppressive activity of $TWIST1^{Hi}$ BM-MSCs in vivo (Fig. 6G). In summary, results reported herein validate *TWIST1* and *TSG6* as biomarkers for quantifying interdonor differences in BM-MSC potency across various assay platforms and disease indications. They also underscore the value of using the CLIP scale to monitor impacts of donor selection and large-scale cell manufacturing on product potency.

MATERIALS AND METHODS

Cell isolation and culture

Primary BM-MSCs were isolated from iliac crest marrow aspirates (Lonza, USA) as previously described (*11*). Briefly, nucleated cells were isolated using a Ficoll-Paque density gradient (Cytiva), suspended in 25 ml of complete culture medium [CCM; α–minimum essential medium supplemented with 2 mM L-glutamine, 17% fetal bovine serum (HyClone), penicillin (100 U/ml), and streptomycin (100 μg/ml)] and expanded in a 15-cm culture dish (Nunclon Delta) at 37°C in 5% CO_2 in a humidified chamber. Media and supplements were purchased from Gibco unless indicated otherwise. Nonadherent cells were discarded by decanting after 24 hours, and the adherent monolayer was washed 2× with phosphate-buffered saline (PBS) and recharged with fresh CCM. Medium changes were performed every 3 to 4 days thereafter, and BM-MSCs were harvested at ~70% confluency with 0.25% trypsin-EDTA, washed in CCM, and plated in 60-mm dishes (500 to 1000 cells/cm^2). The iPSC-derived MSCs were generated as described previously and expanded in a vertical wheel bioreactor (PBS Biotech) while attached to polystyrene microcarriers (*55*, *77*). BM-MSCs transduced with a control retroviral vector MSCV-PIG (Addgene) or one engineered to express a full-length human TWIST1 ORF tagged with HA at its N terminus (HATW1) were used to conduct ChIP analysis (*29*). CFU-Fs were quantified as described previously (*29*). Alternatively, frozen vials of passage 1 BM-MSCs were obtained from the Institute for Regenerative Medicine, Texas A&M University School of Medicine, and the cells were

cultured as previously described (*31*). Where indicated, BM-MSCs were plated at 500 cells/cm^2 and cultured with the CCM containing various concentrations of recombinant human TGF-β2 (R&D Systems) or SB431542 (Sigma-Aldrich) for 4 days with medium changes on day 2. Where indicated, scrambled or TWIST1-, TSG6-, and TGF-β2-specific siRNAs (10 nM; Santa Cruz Biotechnology Inc.) or TSG6 or control plasmids (0.1 to 0.5 μg per well in a six-well plate) (*38*) were transfected into BM-MSC using Lipofectamine RNAiMAX or 2000 (Life Technologies), respectively, according to the manufacturer's protocol, and after 24 to 48 hours, cells were harvested and used for analysis.

TSG6 promoter cloning and mutagenesis

The promoter region of TSG6 was amplified via polymerase chain reaction (PCR) using Q5 High-Fidelity DNA polymerase (New England Biolabs) from genomic DNA extracted from BM-MSCs using the Zymo Quick-DNA kit (Zymo Research). The pGL4.10 [luc2] vector (Promega) was subjected to digestion with Eco RV and Hind III. The amplified PCR product was digested with Hind III and ligated into the pGL4.10[luc2] vector to produce TSG6-pGL4.10[luc2]. The TSG6 promoter site has four canonical Eboxes, which were individually mutated via inverse site-directed mutagenesis. This was achieved by creating forward primers that contained the mutated Ebox site, along with an end-to-end reverse primer to PCR-amplify a mutated vector directly from TSG6-pGL4.10[luc2]. Dpn I was used to cleave the parental, unmutated TSG6-pGL4.10[luc2], and following self-ligation of the PCR product, DH10b bacteria (Life Technologies) were transformed with the resulting DNA to generate Ebox-mutated TSG6-pGL4.10 [luc2] clones. These clones were used for subsequent luciferase assays. Primers used were as follows: *TSG6* promoter forward, 5′ACAAAGGAAGAGGAAAGTTTGG3′ and reverse, 5′AAGCTT ATCGTCAGTTGTAGTGAAGTAA3′; *TSG6* Ebox1 mutant forward, 5′GTTGCCAATGAAAATTAGTCAGAGGATTTG3′ and reverse, 5′CAAAACTAAGGAGATAGAATGATC3′; *TSG6* Ebox2 mutant forward, 5′GCTGACCTCAAAAATTAAAAAAACTATT TAAAAGATGTGG3′ and reverse, 5′AAGTACTCTCCAATGGCA TTTTC3′; *TSG6* Ebox3 mutant forward, 5′ATGT GGAAACAAAATTTTTCAGTCACATTTC3′ and reverse, 3′CTTTTAAATAGTTTTTTTCAACTGTG3′; and *TSG6* Ebox4 mutant forward, 5′TACTTCACTAAAAATTACGATATCAAGCT TGGCAATC3′ and reverse, 5′ACAGCCTGTTAGGGGCTG3′.

TSG6 promoter luciferase assays

To evaluate the inhibitory effect of TWIST1 on TSG6, human embryonic kidney–293 cells were initially transfected with either TSG6-pGL4.10[luc2] or one of four Ebox-mutated TSG6-pGL4.10 [luc2] vectors. Subsequently, the cells were divided into two groups and transfected with either pMSCV-Pig-HA-TWIST1 or a pMSCV-Pig empty vector control. After a 48-hour incubation, luciferase expression was determined using the Dual-Glo Luciferase Reporter System (Promega). The cells were lysed using the Dual-Glo assay reagent, and after a 5-min incubation at room temperature, the luminescence was measured via plate reader (BioTek). The level of luminescence was quantified as a reduction in luminescence in the TWIST1 transfected sample compared to the empty vector control.

Chromatin immunoprecipitation

ChIP was performed according to the manufacturer′s protocol using the ChIP-IT Express kit (Active Motif). Briefly, ~5 × 10^6 HATW1 or MSCV-Pig cells were fixed in a monolayer with 1% paraformaldehyde, quenched with glycine, then gently lifted by scraping, and homogenized with a Dounce homogenizer in manufacturer-provided lysis solution on ice to release the fixed chromatin. Fixed chromatin samples were concentrated in two volumes of ~300-μl shearing buffer, sonicated with a 1/8-inch probe (Qsonica) on ice for five pulses of 20 s at 25% power at 30-s intervals. Shearing was empirically optimized to produce ~500bae pair fragments. Immunoprecipitation reactions (200 μl) were performed overnight on chromatin samples (15 μg) using the manufacturer-provided protein A beads and anti-HA tag antibody HA-7X (sc-7932X, Santa Cruz Biotechnology). Using kit-provided buffers, Protein A beads were washed on a magnetic stand, and the captured chromatin was subsequently eluted. Samples were cleaned up with Proteinase K followed by phenol chloroform extraction. Protein lysates were prepared from HATW1 or MSCV-Pig cell monolayers using NP-40 lysis buffer, and protein concentrations were determined using the Pierce BCA Protein Assay Kit (Thermo Fisher Scientific). Protein samples (20 μg) were prepared in SDS sample buffer containing 5% β-mercaptoethanol, denatured at 95°C for 10 min and electrophoresed on 10% SDS–polyacrylamide gel electrophoresis gels using SDS Running Buffer (Bio-Rad). Transfer papers and 0.45-μm polyvinylidene difluoride (PVDF) membranes were washed with tris-buffered saline (TBS) containing 10% methanol, and the same buffer was used for transfers. Transfer was conducted for 30 min using a semidry rig. Membranes were washed with TBS, and transfer efficiency was assessed with Ponceau Red, which was washed off with TBST. The membrane was blocked for 2 hours at room temperature using nonfat dry milk reconstituted in TBST. Proteins were probed with an anti–HA-peroxidase high affinity antibody (3F10) at a 1:500 dilution for 1 hour at room temperature. Labeled bands were visualized using the SuperSignal West Pico PLUS Chemiluminescent Substrate (Thermo Fisher Scientific, 34577) to expose film.

Quantitative reverse transcription PCR

Total RNA was isolated using the Zymo Quick-RNA Miniprep Kit (R1054, Zymo), converted to cDNA using the qScript cDNA synthesis kit (Quantabio), and amplified by PCR using the POWER SYBR Green PCR Master Mix (Thermo Fisher Scientific) and *TWIST1*, *FGFR2IIIc*, *IDO1*, or *GAPDH* primer sets according to the manufacturer′s instructions. In addition, the following TaqMan probe/primer sets (Thermo Fisher Scientific) were used for PCR amplification using the TaqMan Fast Master Mix (Thermo Fisher Scientific): human *TSG6*, *CD24*, *MGP*, *CXCL6*, *FGF7*, *TGF-β2*, *OXTR*, *CRISPLD2*, *PTX3*, *IL-18*, and *GAPDH*. Reactions were performed on a 7900 HT sequence detector (Applied Biosystems), and transcript levels were quantified using the relative Ct method by using *GAPDH* as an internal control.

Western blot

MSCs were washed 2× with ice-cold PBS and collected in radioimmunoprecipitation assay buffer [50 mM tris-Cl (pH 7.4), 150 mM NaCl, 1% NP-40, 0.5% sodium deoxycholate, and 0.1% SDS] by gently scraping. Lysates were cleared by centrifugation at 12,000*g* for 20 min, and their protein content was measured using the

Bradford method (Bio-Rad). Protein samples were suspended in 4× NuPAGE LDS Sample Buffer, heated for 3 min at 95°C, and separated by electrophoresis on NuPAGE 4 to 12% bis-tris polyacrylamide gels (Invitrogen). Proteins were transferred to PVDF membranes, incubated with TBST [10 mM tris (pH 8.0), 150 mM NaCl, and 0.1% Tween 20] and 5% nonfat dry milk (Bio-Rad) for 1 hour at room temperature, rinsed in TBST, and incubated overnight at 4°C in TBST containing 5% bovine serum albumin with a TWIST1 antibody (E7E2G, Cell Signaling Technology) and glyceraldehyde-3-phosphate dehydrogenase (GAPDH; sc-32233, Santa Cruz Biotechnology).

Adoptive transfer T1D mouse model

Female nonobese diabetic (NOD)/LtJ (12 weeks old) and NOD/*scid* mice (7 weeks old) were used for an adoptive transfer model of T1D. All mice were purchased from the Jackson Laboratory (Bar Harbor, ME) and cared for at the Texas A&M University Comparative Medicine Program under a protocol approved by the Institutional Animal Care and Use Committee. To induce an adoptive transfer in the T1D model, 10^7 splenocytes from prediabetic 12-week-old female NOD mice were intravenously injected into 7-week-old female NOD/*scid* mice. BM-MSCs (1×10^6) or vehicle control were injected intravenously twice at 15 min after splenocyte transfer and on day 4 thereafter. Blood glucose levels were measured twice a week by tail bleeding according to National Institutes of Health guidelines, and diabetes in mice was defined as having the two consecutive glycemic values above 250 mg/dl.

Microarray

RNA was isolated from BM-MSCs with RNeasy Mini Kit (QIAGEN) and assayed on human microarray (HOA 7.1; OneArray, San Diego, CA).

Endothelial tubule formation and invasion assays

HUVECs (30,000 cells/well) were seeded on top of growth factor reduced Matrigel (BD Biosciences) in a 96-well plate with Medium 200PRF (Invitrogen) supplemented with CM from BM-MSCs and incubated for 6 hours. Tube formation was analyzed and quantified using the WIMASIS software (Onimagin Technologies SCA, Spain). For invasion assays, HUVECs (30,000 cells) were seeded on type 1 collagen matrices (2.5 mg/ml; Pel-Freez Biologicals, AK), which was supplemented with BM-MSC CM (×1) and 1 μM sphingosine-1-phosphate (Avanti Polar Lipids, AL). Cells were allowed to invade into type 1 collagen matrices in the presence of HUVEC media containing M199 medium (Gibco, MA) supplemented with 1× RSII, ascorbic acid, and basic fibroblast growth factor (40 ng/ml) and vascular endothelial growth factor (40 ng/ml; R&D Systems, MN). Following overnight invasion, the cells were fixed in 3% glutaraldehyde in PBS overnight, and gels were stained with 10 μM 4′,6-diamidino-2-phenylindole, and confocal images were captured with a Nikon Eclipse TI. Nuclear invasion distance was quantified using NIS Elements AR software of images rendered in the volume view with Alpha depth coding selected. Distance measurements were taken from the monolayer to the bottom of each cell nucleus.

ROS assay

BM-MSCs were plated at 200 cells/cm^2 and cultured for 5 days with CCM, and the total ROS levels in cells was measured by flow cytometry with a commercial kit (Abcam, Waltham, MA).

Osteogenic differentiation

BM-MSCs were cultured in CCM supplemented with 10 nM dexamethasone, 10 mM β-glycerophosphate (Sigma-Aldrich), and 50 μM ascorbate-2-phosphate (Sigma-Aldrich) for 11 to 14 days with medium changes every 2 to 3 days. Cell monolayers were then fixed with 10% formalin for 30 min and stained with 2% Alizarin Red S. For calcium quantification, an Alizarin Red–based assay was used as described previously (*38*).

Mouse model of peritonitis and measurements of inflammation

To induce inflammation in 8-week-old male C57BL/6 mice (the Jackson Laboratory), 1 ml of Zymosan A solution (1 mg/ml; Sigma-Aldrich) was administered by intraperitoneal injection. After 15 min, mice were administered PBS, dexamethasone (1.5 mg/kg; Sigma-Aldrich), or iPSC-MSCs (1.5×10^6 cells per mouse) by intraperitoneal injection. Inflammatory exudates were collected by peritoneal lavage at 4 hours after treatment, and the cell-free supernatant was used to measure levels of the proinflammatory mediators by ELISA (mTNF-α, mCXCL1, and mCXCL2; R&D Systems).

Statistical analysis

All data are reported as means ± SD. The statistical significance between two independent experimental groups was assessed using a two-tailed, unpaired Student's t test. The statistical significance among more than two groups was assessed using a one-way analysis of variance (ANOVA) with multiple comparisons evaluated by the Tukey's or Dunnett's test. The log-rank (Mantel-Cox) test was used to determine differences in the survival experience of mice between experimental groups. Linear correlations are reported as the Pearson's r and corresponding P values determined by linear regression. Significance level was set at $P \leq 0.05$.

Supplementary Materials

This PDF file includes:

Figs. S1 to S4

REFERENCES AND NOTES

1. D. J. Prockop, Marrow stromal cells as stem cells for nonhematopoietic tissues. *Science* **276**, 71–74 (1997).
2. T. M. Dexter, L. H. Coutinho, E. Spooncer, C. M. Heyworth, C. P. Daniel, R. Schiro, J. Chang, T. D. Allen, Stromal cells in haemopoiesis. *Ciba Found. Symp.* **148**, 76–86 (1990).
3. E. I. Deryugina, C. E. Muller-Sieburg, Stromal cells in long-term cultures: Keys to the elucidation of hematopoietic development? *Crit. Rev. Immunol.* **13**, 115–150 (1993).
4. A. J. Friedenstein, K. V. Petrakova, A. I. Kurolesova, G. P. Frolova, Heterotopic transplants of bone marrow. *Transplantation* **6**, 230–247 (1968).
5. D. G. Phinney, Biochemical heterogeneity of mesenchymal stem cell populations: Clues to their therapeutic efficacy. *Cell Cycle* **6**, 2884–2889 (2007).
6. D. G. Phinney, K. Hill, C. Michelson, M. DuTreil, C. Hughes, S. Humphries, R. Wilkinson, M. Baddoo, E. Bayly, Biological activities encoded by the murine mesenchymal stem cell transcriptome provide a basis for their developmental potential and broad therapeutic efficacy. *Stem Cells* **24**, 186–198 (2006).

7. R. C. Lai, F. Arslan, M. M. Lee, N. S. K. Sze, A. Choo, T. S. Chen, M. Salto-Tellez, L. Timmers, C. N. Lee, R. M. El Oakley, G. Pasterkamp, D. P. V. de Kleijn, S. K. Lim, Exosome secreted by MSC reduces myocardial ischemia/reperfusion injury. *Stem Cell Res.* **4**, 214–222 (2010).
8. A. Wright, M. L. Arthaud-Day, M. L. Weiss, Therapeutic use of mesenchymal stromal cells: The need for inclusive characterization guidelines to accommodate all tissue sources and species. *Front. Cell Dev. Biol.* **9**, 632717 (2021).
9. W. Wagner, A. D. Ho, Mesenchymal stem cell preparations–Comparing apples and oranges. *Stem Cell Rev.* **3**, 239–248 (2007).
10. S. Zhou, J. S. Greenberger, M. W. Epperly, J. P. Goff, C. Adler, M. S. LeBoff, J. Glowacki, Age-related intrinsic changes in human bone-marrow-derived mesenchymal stem cells and their differentiation to osteoblasts. *Aging Cell* **7**, 335–343 (2008).
11. K. C. Russell, D. G. Phinney, M. R. Lacey, B. L. Barrilleaux, K. E. Meyertholen, K. C. O'Connor, In vitro high-capacity assay to quantify the clonal heterogeneity in trilineage potential of mesenchymal stem cells reveals a complex hierarchy of lineage commitment. *Stem Cells* **28**, 788–798 (2010).
12. K. P. Robb, J. C. Fitzgerald, F. Barry, S. Viswanathan, Mesenchymal stromal cell therapy: Progress in manufacturing and assessments of potency. *Cytotherapy* **21**, 289–306 (2019).
13. S. Viswanathan, A. Keating, R. Deans, P. Hematti, D. Prockop, D. F. Stroncek, G. Stacey, D. J. Weiss, C. Mason, M. S. Rao, Soliciting strategies for developing cell-based reference materials to advance mesenchymal stromal cell research and clinical translation. *Stem Cells Dev.* **23**, 1157–1167 (2014).
14. T. I. van der Spoel, S. J. Jansen, P. Agostoni, E. van Belle, M. Gyöngyösi, J. P. G. Sluijter, M. J. Cramer, P. A. Doevendans, S. A. J. Chamuleau, Human relevance of pre-clinical studies in stem cell therapy: Systematic review and meta-analysis of large animal models of ischaemic heart disease. *Cardiovasc. Res.* **91**, 649–658 (2011).
15. L. von Bahr, B. Sundberg, L. Lönnies, B. Sander, H. Karbach, H. Hägglund, P. Ljungman, B. Gustafsson, H. Karlsson, K. le Blanc, O. Ringdén, Long-term complications, immunologic effects, and role of passage for outcome in mesenchymal stromal cell therapy. *Biol. Blood Marrow Transplant.* **18**, 557–564 (2012).
16. M. Krampera, K. Le Blanc, Mesenchymal stromal cells: Putative microenvironmental modulators become cell therapy. *Cell Stem Cell* **28**, 1708–1725 (2021).
17. S. V. Boregowda, D. G. Phinney, Quantifiable metrics for predicting MSC therapeutic efficacy. *J. Stem Cell Res. Ther.* **6**, 365 (2016).
18. B. Thisse, M. el Messal, F. Perrin-Schmitt, The twist gene: Isolation of a Drosophila zygotic gene necessary for the establishment of dorsoventral pattern. *Nucleic Acids Res.* **15**, 3439–3453 (1987).
19. Y. Wang, D. Q. Chen, M. Y. Chen, K. Y. Ji, D. X. Ma, L. F. Zhou, Endothelial cells by inactivation of VHL gene direct angiogenesis, not vasculogenesis via Twist1 accumulation associated with hemangioblastoma neovascularization. *Sci. Rep.* **7**, 5463 (2017).
20. M. M. Mahmoud, H. R. Kim, R. Xing, S. Hsiao, A. Mammoto, J. Chen, J. Serbanovic-Canic, S. Feng, N. P. Bowden, R. Maguire, M. Ariaans, S. E. Francis, P. D. Weinberg, K. van der Heiden, E. A. Jones, T. J. A. Chico, V. Ridger, P. C. Evans, TWIST1 integrates endothelial responses to flow in vascular dysfunction and atherosclerosis. *Circ. Res.* **119**, 450–462 (2016).
21. T. Mammoto, A. Jiang, E. Jiang, A. Mammoto, Role of Twist1 phosphorylation in angiogenesis and pulmonary fibrosis. *Am. J. Respir. Cell Mol. Biol.* **55**, 633–644 (2016).
22. J. M. Low-Marchelli, V. C. Ardi, E. A. Vizcarra, N. van Rooijen, J. P. Quigley, J. Yang, Twist1 induces CCL2 and recruits macrophages to promote angiogenesis. *Cancer Res.* **73**, 662–671 (2013).
23. N. Wang, J. Yin, N. You, S. Yang, D. Guo, Y. Zhao, Y. Ru, X. Liu, H. Cheng, Q. Ren, T. Cheng, X. Ma, TWIST1 preserves hematopoietic stem cell function via the CACNA1B/Ca^{2+}/mitochondria axis. *Blood* **137**, 2907–2919 (2021).
24. A. Arthur, D. Cakouros, L. Cooper, T. Nguyen, S. Isenmann, A. C. W. Zannettino, C. A. Glackin, S. Gronthos, Twist-1 enhances bone marrow mesenchymal stromal cell support of hematopoiesis by modulating CXCL12 expression. *Stem Cells* **34**, 504–509 (2016).
25. N. Liu, G. A. Garry, S. Li, S. Bezprozvannaya, E. Sanchez-Ortiz, B. Chen, J. M. Shelton, P. Jaichander, R. Bassel-Duby, E. N. Olson, A Twist2-dependent progenitor cell contributes to adult skeletal muscle. *Nat. Cell Biol.* **19**, 202–213 (2017).
26. I. Y. Choi, H. Lim, H. J. Cho, Y. Oh, B. K. Chou, H. Bai, L. Cheng, Y. J. Kim, S. H. Hyun, H. Kim, J. H. Shin, G. Lee, Transcriptional landscape of myogenesis from human pluripotent stem cells reveals a key role of TWIST1 in maintenance of skeletal muscle progenitors. *eLife* **9**, e46981 (2020).
27. C.-Y. Dong, X.-Y. Liu, N. Wang, L.-N. Wang, B.-X. Yang, Q. Ren, H.-Y. Liang, X.-T. Ma, Twist-1, a novel regulator of hematopoietic stem cell self-renewal and myeloid lineage development. *Stem Cells* **32**, 3173–3182 (2014).
28. D. Šošić, J. A. Richardson, K. Yu, D. M. Ornitz, E. N. Olson, Twist regulates cytokine gene expression through a negative feedback loop that represses NF-κB activity. *Cell* **112**, 169–180 (2003).
29. S. V. Boregowda, V. Krishnappa, C. L. Haga, L. A. Ortiz, D. G. Phinney, A clinical indications prediction scale based on TWIST1 for human mesenchymal stem cells. *EBioMedicine* **4**, 62–73 (2016).
30. K. P. Robb, J. Audet, R. Gandhi, S. Viswanathan, Putative critical quality attribute matrix identifies mesenchymal stromal cells with potent immunomodulatory and angiogenic "fitness" ranges in response to culture process parameters. *Front. Immunol.* **13**, 972095 (2022).
31. R. H. Lee, A. A. Pulin, M. J. Seo, D. J. Kota, J. Ylostalo, B. L. Larson, L. Semprun-Prieto, P. Delafontaine, D. J. Prockop, Intravenous hMSCs improve myocardial infarction in mice because cells embolized in lung are activated to secrete the anti-inflammatory protein TSG-6. *Cell Stem Cell* **5**, 54–63 (2009).
32. N. Wang, Y. Shao, Y. Mei, L. Zhang, Q. Li, D. Li, S. Shi, Q. Hong, H. Lin, X. Chen, Novel mechanism for mesenchymal stem cells in attenuating peritoneal adhesion: Accumulating in the lung and secreting tumor necrosis factor α-stimulating gene-6. *Stem Cell Res. Ther.* **3**, 51 (2012).
33. Z. He, J. Hua, D. Qian, J. Gong, S. Lin, C. Xu, G. Wei, H. Meng, T. Yang, B. Zhou, Z. Song, Intravenous hMSCs ameliorate acute pancreatitis in mice via secretion of tumor necrosis factor-α stimulated gene/protein 6. *Sci. Rep.* **6**, 38438 (2016).
34. H. Choi, R. H. Lee, N. Bazhanov, J. Y. Oh, D. J. Prockop, Anti-inflammatory protein TSG-6 secreted by activated MSCs attenuates zymosan-induced mouse peritonitis by decreasing TLR2/NF-κB signaling in resident macrophages. *Blood* **118**, 330–338 (2011).
35. E. Sala, M. Genua, L. Petti, A. Anselmo, V. Arena, J. Cibella, L. Zanotti, S. D'Alessio, F. Scaldaferri, G. Luca, I. Arato, R. Calafiore, A. Sgambato, S. Rutella, M. Locati, S. Danese, S. Vetrano, Mesenchymal stem cells reduce colitis in mice via release of TSG6, independently of their localization to the intestine. *Gastroenterology* **149**, 163–176.e20 (2015).
36. W.-J. Song, Q. Li, M.-O. Ryu, J.-O. Ahn, D. H. Bhang, Y. C. Jung, H.-Y. Youn, TSG-6 secreted by human adipose tissue-derived mesenchymal stem cells ameliorates DSS-induced colitis by inducing M2 macrophage polarization in mice. *Sci. Rep.* **7**, 5187 (2017).
37. H. B. Song, S. Y. Park, J. H. Ko, J. W. Park, C. H. Yoon, D. H. Kim, J. H. Kim, M. K. Kim, R. H. Lee, D. J. Prockop, J. Y. Oh, Mesenchymal stromal cells inhibit inflammatory lymphangiogenesis in the cornea by suppressing macrophage in a TSG-6-dependent manner. *Mol. Ther.* **26**, 162–172 (2018).
38. R. H. Lee, J. M. Yu, A. M. Foskett, G. Peltier, J. C. Reneau, N. Bazhanov, J. Y. Oh, D. J. Prockop, TSG-6 as a biomarker to predict efficacy of human mesenchymal stem/progenitor cells (hMSCs) in modulating sterile inflammation in vivo. *Proc. Natl. Acad. Sci. U.S.A.* **111**, 16766–16771 (2014).
39. Z. A. Yochum, J. Cades, L. Mazzacurati, N. M. Neumann, S. K. Khetarpal, S. Chatterjee, H. Wang, M. A. Attar, E. H. B. Huang, S. N. Chatley, K. Nugent, A. Somasundaram, J. A. Engh, A. J. Ewald, Y. J. Cho, C. M. Rudin, P. T. Tran, T. F. Burns, A first-in-class TWIST1 inhibitor with activity in oncogene-driven lung cancer. *Mol. Cancer Res.* **15**, 1764–1776 (2017).
40. J. Fan, S. Li, D. Wang, MicroRNA-149 suppresses osteogenic differentiation of mesenchymal stem cells via inhibition of AKT1-dependent Twist1 phosphorylation. *Cell Death Discov.* **8**, 2 (2022).
41. H. Miraoui, N. Severe, P. Vaudin, J. C. Pages, P. J. Marie, Molecular silencing of Twist1 enhances osteogenic differentiation of murine mesenchymal stem cells: Implication of FGFR2 signaling. *J. Cell. Biochem.* **110**, 1147–1154 (2010).
42. N. Quarto, K. Senarath-Yapa, A. Renda, M. T. Longaker, TWIST1 silencing enhances in vitro and in vivo osteogenic differentiation of human adipose-derived stem cells by triggering activation of BMP-ERK/FGF signaling and TAZ upregulation. *Stem Cells* **33**, 833–847 (2015).
43. S. V. Boregowda, S. Ghoshal, C. N. Booker, V. Krishnappa, A. Chakraborty, D. G. Phinney, IP6K1 reduces mesenchymal stem/stromal cell fitness and potentiates high fat diet-induced skeletal involution. *Stem Cells* **35**, 1973–1983 (2017).
44. N. Floc'h, J. Kolodziejski, L. Akkari, Y. Simonin, S. Ansieau, A. Puisieux, U. Hibner, P. Lassus, Modulation of oxidative stress by twist oncoproteins. *PLOS ONE* **8**, e72490 (2013).
45. J. Krstić, D. Trivanović, S. Mojsilović, J. F. Santibanez, Transforming growth factor-beta and oxidative stress interplay: Implications in tumorigenesis and cancer progression. *Oxid. Med. Cell. Longev.* **2015**, 654594 (2015).
46. H.-Y. Chen, H.-C. Chou, Y.-J. Ho, S.-J. Chang, E.-C. Liao, Y.-S. Wei, M.-W. Lin, Y.-S. Wang, Y.-A. Chien, X.-R. Yu, H.-Y. Kung, C.-C. Yang, J.-Y. Chen, H.-L. Chan, M.-L. Ko, Characterization of TGF-β by induced oxidative stress in human trabecular meshwork cells. *Antioxidants* **10**, 107 (2021).
47. R. M. Liu, L. P. Desai, Reciprocal regulation of TGF-β and reactive oxygen species: A perverse cycle for fibrosis. *Redox Biol.* **6**, 565–577 (2015).
48. F. Verrecchia, A. Mauviel, Transforming growth factor-β signaling through the Smad pathway: Role in extracellular matrix gene expression and regulation. *J. Invest. Dermatol.* **118**, 211–215 (2002).
49. F. Liu, J. Xie, X. Zhang, Z. Wu, S. Zhang, M. Xue, J. Chen, Y. Yang, H. Qiu, Overexpressing TGF-β1 in mesenchymal stem cells attenuates organ dysfunction during CLP-induced septic mice by reducing macrophage-driven inflammation. *Stem Cell Res. Ther.* **11**, 378 (2020).

50. K. Lynch, O. Treacy, X. Chen, N. Murphy, P. Lohan, M. N. Islam, E. Donohoe, M. D. Griffin, L. Watson, S. McLoughlin, G. O'Malley, A. E. Ryan, T. Ritter, TGF-β1-licensed murine MSCs show superior therapeutic efficacy in modulating corneal allograft immune rejection in vivo. *Mol. Ther.* **28**, 2023–2043 (2020).
51. C. Xu, P. Yu, X. Han, L. du, J. Gan, Y. Wang, Y. Shi, TGF-β promotes immune responses in the presence of mesenchymal stem cells. *J. Immunol.* **192**, 103–109 (2014).
52. G. J. Inman, F. J. Nicolás, J. F. Callahan, J. D. Harling, L. M. Gaster, A. D. Reith, N. J. Laping, C. S. Hill, SB-431542 is a potent and specific inhibitor of transforming growth factor-beta superfamily type I activin receptor-like kinase (ALK) receptors ALK4, ALK5, and ALK7. *Mol. Pharmacol.* **62**, 65–74 (2002).
53. Y. S. Chen, R. A. Pelekanos, R. L. Ellis, R. Horne, E. J. Wolvetang, N. M. Fisk, Small molecule mesengenic induction of human induced pluripotent stem cells to generate mesenchymal stem/stromal cells. *Stem Cells Transl. Med.* **1**, 83–95 (2012).
54. A. Leyendecker Jr., TGF-β inhibitor SB431542 promotes the differentiation of induced pluripotent stem cells and embryonic stem cells into mesenchymal-like cells. *Stem Cells Int.* **2018**, 7878201 (2018).
55. Q. Zhao, C. A. Gregory, R. H. Lee, R. L. Reger, L. Qin, B. Hai, M. S. Park, N. Yoon, B. Clough, E. McNeill, D. J. Prockop, F. Liu, MSCs derived from iPSCs with a modified protocol are tumor-tropic but have much less potential to promote tumors than bone marrow MSCs. *Proc. Natl. Acad. Sci. U.S.A.* **112**, 530–535 (2015).
56. E. P. McNeill, S. Zeitouni, S. Pan, A. Haskell, M. Cesarek, D. Tahan, B. H. Clough, U. Krause, L. K. Dobson, M. Garcia, C. Kung, Q. Zhao, W. B. Saunders, F. Liu, R. Kaunas, C. A. Gregory, Characterization of a pluripotent stem cell-derived matrix with powerful osteoregenerative capabilities. *Nat. Commun.* **11**, 3025 (2020).
57. Y. I. Yun, S. Y. Park, H. J. Lee, J. H. Ko, M. K. Kim, W. R. Wee, R. L. Reger, C. A. Gregory, H. Choi, S. F. Fulcher, D. J. Prockop, J. Y. Oh, Comparison of the anti-inflammatory effects of induced pluripotent stem cell-derived and bone marrow-derived mesenchymal stromal cells in a murine model of corneal injury. *Cytotherapy* **19**, 28–35 (2017).
58. Y. J. Wang, L. Y. Zheng, Z. F. Wang, R. Song, L. Yang, Y. H. Geng, F. Mei, Y. T. Xie, L. Chen, D. G. Liu, X. H. Li, Y. L. Sun, X. X. Tian, W. G. Fang, Associations of gene-wide SNPs in SNAI1 and TWIST1 with breast cancer and ovarian cancer susceptibility among Chinese Han women. *Oncol. Rep.* **40**, 3573–3584 (2018).
59. S. Romero, M. Musleh, M. Bustamante, J. Stambuk, R. Pisano, E. Lanzarini, H. Chiong, J. Rojas, V. G. Castro, L. Jara, Z. Berger, P. Gonzalez-Hormazabal, Polymorphisms in *TWIST1* and *ZEB1* are associated with prognosis of gastric cancer patients. *Anticancer Res* **38**, 3871–3877 (2018).
60. J. Y. Hwang, S. Y. Kim, S. H. Lee, G. S. Kim, M. J. Go, S. E. Kim, H. C. Kim, H. D. Shin, B. L. Park, T. H. Kim, J. M. Hong, E. K. Park, H. L. Kim, J. Y. Lee, J. M. Koh, Association of TWIST1 gene polymorphisms with bone mineral density in postmenopausal women. *Osteoporos. Int.* **21**, 757–764 (2010).
61. D. G. Phinney, M. Di Giuseppe, J. Njah, E. Sala, S. Shiva, C. M. St Croix, D. B. Stolz, S. C. Watkins, Y. P. Di, G. D. Leikauf, J. Kolls, D. W. H. Riches, G. Deiuliis, N. Kaminski, S. V. Boregowda, D. H. McKenna, L. A. Ortiz, Mesenchymal stem cells use extracellular vesicles to outsource mitophagy and shuttle microRNAs. *Nat. Commun.* **6**, 8472 (2015).
62. J. M. Hare, J. E. Fishman, G. Gerstenblith, D. L. DiFede Velazquez, J. P. Zambrano, V. Y. Suncion, M. Tracy, E. Ghersin, P. V. Johnston, J. A. Brinker, E. Breton, J. Davis-Sproul, J. Byrnes, R. George, A. Lardo, I. H. Schulman, A. M. Mendizabal, M. H. Lowery, D. Rouy, P. Altman, C. Wong Po Foo, P. Ruiz, A. Amador, J. da Silva, I. K. McNiece, A. W. Heldman, Comparison of allogeneic vs autologous bone marrow-derived mesenchymal stem cells delivered by transendocardial injection in patients with ischemic cardiomyopathy: The POSEIDON randomized trial. *JAMA* **308**, 2369–2379 (2012).
63. J. M. Hare, D. L. DiFede, A. C. Rieger, V. Florea, A. M. Landin, J. el-Khorazaty, A. Khan, M. Mushtaq, M. H. Lowery, J. J. Byrnes, R. C. Hendel, M. G. Cohen, C. E. Alfonso, K. Valasaki, M. V. Pujol, S. Golpanian, E. Ghersin, J. E. Fishman, P. Pattany, S. A. Gomes, C. Delgado, R. Miki, F. Abuzeid, M. Vidro-Casiano, C. Premer, A. Medina, V. Porras, K. E. Hatzistergos, E. Anderson, A. Mendizabal, R. Mitrani, A. W. Heldman, Randomized comparison of allogeneic versus autologous mesenchymal stem cells for nonischemic dilated cardiomyopathy: POSEIDON-DCM trial. *J. Am. Coll. Cardiol.* **69**, 526–537 (2017).
64. J. Bartunek, A. Behfar, D. Dolatabadi, M. Vanderheyden, M. Ostojic, J. Dens, B. el Nakadi, M. Banovic, B. Beleslin, M. Vrolix, V. Legrand, C. Vrints, J. L. Vanoverschelde, R. Crespo-Diaz, C. Homsy, M. Tendera, S. Waldman, W. Wijns, A. Terzic, Cardiopoietic stem cell therapy in heart failure: The C-CURE (Cardiopoietic stem Cell therapy in heart failURE) multicenter randomized trial with lineage-specified biologics. *J. Am. Coll. Cardiol.* **61**, 2329–2338 (2013).
65. A. W. Heldman, D. L. DiFede, J. E. Fishman, J. P. Zambrano, B. H. Trachtenberg, V. Karantalis, M. Mushtaq, A. R. Williams, V. Y. Suncion, I. K. McNiece, E. Ghersin, V. Soto, G. Lopera, R. Miki, H. Willens, R. Hendel, R. Mitrani, P. Pattany, G. Feigenbaum, B. Oskouei, J. Byrnes, M. H. Lowery, J. Sierra, M. V. Pujol, C. Delgado, P. J. Gonzalez, J. E. Rodriguez, L. L. Bagno, D. Rouy, P. Altman, C. W. P. Foo, J. da Silva, E. Anderson, R. Schwarz, A. Mendizabal, J. M. Hare, Transendocardial mesenchymal stem cells and mononuclear bone marrow cells for ischemic cardiomyopathy: The TAC-HFT randomized trial. *JAMA* **311**, 62–73 (2014).
66. M. E. Bowdish, C. E. Barkauskas, J. R. Overbey, R. L. Gottlieb, K. Osman, A. Duggal, M. E. Marks, J. Hupf, E. Fernandes, B. G. Leshnower, J. L. Golob, A. Iribarne, A. J. Rassias, E. G. Moquete, K. O'Sullivan, H. L. Chang, J. B. Williams, S. Parnia, N. C. Patel, N. D. Desai, A. M. Vekstein, B. A. Hollister, T. Possemato, C. Romero, P. C. Hou, E. Burke, J. Hayes, F. Grossman, S. Itescu, M. Gillinov, F. D. Pagani, P. T. O'Gara, M. J. Mack, P. K. Smith, E. Bagiella, A. J. Moskowitz, A. C. Gelijns, A randomized trial of mesenchymal stromal cells for moderate to severe acute respiratory distress syndrome from COVID-19. *Am. J. Respir. Crit. Care Med.* **207**, 261–270 (2023).
67. A. Monsel, C. Hauw-Berlemont, M. Mebarki, N. Heming, J. Mayaux, O. N. Tchoumba, J.-L. Diehl, A. Demoule, D. Annane, C. Marois, S. Demeret, E. Weiss, G. Voiriot, M. Fartoukh, J.-M. Constantin, B. Mégarbane, G. Plantefève, S. Malard-Castagnet, S. Burrel, M. Rosenzwajg, N. Tchitchek, H. Boucher-Pillet, G. Churlaud, A. Cras, C. Maheux, C. Pezzana, M. H. Diallo, J. Ropers, P. Menasché, J. Larghero; APHP STROMA–Co V- Collaborative Research Group, Treatment of COVID-19-associated ARDS with mesenchymal stromal cells: A multicenter randomized double-blind trial. *Crit. Care* **26**, 48 (2022).
68. M. A. Matthay, C. S. Calfee, H. Zhuo, B. T. Thompson, J. G. Wilson, J. E. Levitt, A. J. Rogers, J. E. Gotts, J. P. Wiener-Kronish, E. K. Bajwa, M. P. Donahoe, B. J. McVerry, L. A. Ortiz, M. Exline, J. W. Christman, J. Abbott, K. L. Delucchi, L. Caballero, M. McMillan, D. H. McKenna, K. D. Liu, Treatment with allogeneic mesenchymal stromal cells for moderate to severe acute respiratory distress syndrome (START study): A randomised phase 2a safety trial. *Lancet Respir. Med.* **7**, 154–162 (2019).
69. K. Le Blanc, F. Frassoni, L. Ball, F. Locatelli, H. Roelofs, I. Lewis, E. Lanino, B. Sundberg, M. E. Bernardo, M. Remberger, G. Dini, R. M. Egeler, A. Bacigalupo, W. Fibbe, O. Ringdén; Developmental Committee of the European Group for Blood and Marrow Transplantation, Mesenchymal stem cells for treatment of steroid-resistant, severe, acute graft-versus-host disease: A phase II study. *Lancet* **371**, 1579–1586 (2008).
70. J. Kurtzberg, S. Prockop, P. Teira, H. Bittencourt, V. Lewis, K. W. Chan, B. Horn, L. Yu, J. A. Talano, E. Nemecek, C. R. Mills, S. Chaudhury, Allogeneic human mesenchymal stem cell therapy (remestemcel-L, Prochymal) as a rescue agent for severe refractory acute graft-versus-host disease in pediatric patients. *Biol. Blood Marrow Transplant.* **20**, 229–235 (2014).
71. J. Kurtzberg, H. Abdel-Azim, P. Carpenter, S. Chaudhury, B. Horn, K. Mahadeo, E. Nemecek, S. Neudorf, V. Prasad, S. Prockop, T. Quigg, P. Satwani, A. Cheng, E. Burke, J. Hayes, D. Skerrett; MSB-GVHD/ Study Group, A phase 3, single-arm, prospective study of remestemcel-l, ex vivo culture-expanded adult human mesenchymal stromal cells for the treatment of pediatric patients who failed to respond to steroid treatment for acute graft-versus-host disease. *Biol. Blood Marrow Transplant.* **26**, 845–854 (2020).
72. M. von Bonin, F. Stölzel, A. Goedecke, K. Richter, N. Wuschek, K. Hölig, U. Platzbecker, T. Illmer, M. Schaich, J. Schetelig, A. Kiani, R. Ordemann, G. Ehninger, M. Schmitz, M. Bornhäuser, Treatment of refractory acute GVHD with third-party MSC expanded in platelet lysate-containing medium. *Bone Marrow Transplant.* **43**, 245–251 (2009).
73. G. Lucchini, M. Introna, E. Dander, A. Rovelli, A. Balduzzi, S. Bonanomi, A. Salvadè, C. Capelli, D. Belotti, G. Gaipa, P. Perseghin, P. Vinci, E. Lanino, P. Chiusolo, M. G. Orofino, S. Marktel, J. Golay, A. Rambaldi, A. Biondi, G. D'Amico, E. Biagi, Platelet-lysate-expanded mesenchymal stromal cells as a salvage therapy for severe resistant graft-versus-host disease in a pediatric population. *Biol. Blood Marrow Transplant.* **16**, 1293–1301 (2010).
74. F. McKinnirey, B. Herbert, G. Vesey, S. McCracken, Immune modulation via adipose derived mesenchymal stem cells is driven by donor sex in vitro. *Sci. Rep.* **11**, 12454 (2021).
75. M. Krampera, L. Cosmi, R. Angeli, A. Pasini, F. Liotta, A. Andreini, V. Santarlasci, B. Mazzinghi, G. Pizzolo, F. Vinante, P. Romagnani, E. Maggi, S. Romagnani, F. Annunziato, Role for interferon-γ in the immunomodulatory activity of human bone marrow mesenchymal stem cells. *Stem Cells* **24**, 386–398 (2006).
76. G. Ren, L. Zhang, X. Zhao, G. Xu, Y. Zhang, A. I. Roberts, R. C. Zhao, Y. Shi, Mesenchymal stem cell-mediated immunosuppression occurs via concerted action of chemokines and nitric oxide. *Cell Stem Cell* **2**, 141–150 (2008).
77. R. E. Rogers, A. Haskell, B. P. White, S. Dalal, M. Lopez, D. Tahan, S. Pan, G. Kaur, H. Kim, H. Barreda, S. L. Woodard, O. R. Benavides, J. Dai, Q. Zhao, K. C. Maitland, A. Han, Z. L. Nikolov, F. Liu, R. H. Lee, C. A. Gregory, R. Kaunas, A scalable system for generation of mesenchymal stem cells derived from induced pluripotent cells employing bioreactors and degradable microcarriers. *Stem Cells Transl. Med.* **10**, 1650–1665 (2021).

Acknowledgments: We thank F. Liu, Texas A&M University School of Medicine, for providing iPSC-MSCs. **Funding:** This work was supported by funding from the NIH grants R01 HL144089 (D.G.P.) and R01 EY029350 (R.H.L.) and an X-Grant from the Texas A&M University President's Excellence Fund (C.A.G. and R.H.L.). **Author contributions:** Conceptualization: D.G.P., R.H.L., L. A.O., and S.V.B. Methodology: R.H.L., S.V.B., T.S-K., E.B., C.L.H., K.J.B., C.A.A., C.A.G., and A.H. Formal analysis: D.G.P., R.H.L., C.L.H., S.V.B., K.J.B., and C.A.A. Investigation: R.H.L., S.V.B., T.S-K., E. B., C.A.G., and A.H. Visualization: D.G.P., R.H.L., and C.L.H. Funding acquisition: D.G.P., R.H.L., and

C.A.G. Supervision: D.G.P., R.H.L., and K.J.B. Writing (original draft): D.G.P. and R.H.L. Writing (review and editing): D.G.P., R.H.L., S.V.B., C.L.H., C.A.G., and K.J.B. **Competing interests:** The authors declare that they have no competing interests. **Data and materials availability:** All data needed to evaluate the conclusions in the paper are present in the paper and/or the Supplementary Materials.

Submitted 12 April 2023
Accepted 11 October 2023
Published 10 November 2023
10.1126/sciadv.adi2387